1521-009X/50/9/1272–1286$35.00
DRUG METABOLISM AND DISPOSITION

dx.doi.org/10.1124/dmd.122.000883
Drug Metab Dispos 50:1272–1286, September 2022



# An Improved Method for Cytochrome P450 Reaction Phenotyping Using a Sequential Qualitative-Then-Quantitative Approach

Angela C. Doran, Alyssa L. Dantonio, Gabrielle M. Gualtieri, Amanda Balesano, Connor Landers, Woodrow Burchett, Theunis C. Goosen, and R. Scott Obach

*Medicine Design, Pfizer Worldwide Research, Development and Medical, Groton, Connecticut*

Received March 2, 2022; accepted May 11, 2022

## ABSTRACT

**Cytochrome P450 reaction phenotyping to determine the fraction of metabolism ($f_m$) values for individual enzymes is a standard study in the evaluation of a new drug. However, there are technical challenges in these studies caused by shortcomings in the selectivity of P450 inhibitors and unreliable scaling procedures for recombinant P450 (rCYP) data. In this investigation, a two-step "qualitative-then-quantitative" approach to P450 reaction phenotyping is described. In the first step, each rCYP is tested qualitatively for potential to generate metabolites. In the second step, selective inhibitors for the P450s identified in step 1 are tested for their effects on metabolism using full inhibition curves. Forty-eight drugs were evaluated in step 1 and there were no examples of missing an enzyme important to in vivo clearance. Five drugs (escitalopram, fluvastatin, pioglitazone, propranolol, and risperidone) were selected for full phenotyping in step 2 to determine $f_m$ values, with findings compared with $f_m$ values estimated from single-inhibitor concentration data and rCYP with intersystem extrapolation factor corrections. The two-step approach yielded $f_m$ values for major drug-clearing enzymes that are close to those estimated from clinical data: escitalopram and CYP2C19 (0.42 versus 0.36–0.82), fluvastatin and CYP2C9 (0.76 versus 0.76), pioglitazone and CYP2C8 (0.72 versus 0.73), propranolol and CYP2D6 (0.68 versus 0.37–0.56) and risperidone and CYP2D6 (0.60 versus 0.66–0.88). Reaction phenotyping data generated in this fashion should offer better input to physiologically based pharmacokinetic models for prediction of drug-drug interaction and impact of genetic polymorphisms on drug clearance. The qualitative-then-quantitative approach is proposed as a replacement to standard reaction phenotyping strategies.**

## SIGNIFICANCE STATEMENT

**Cytochrome P450 reaction phenotyping is important for projecting drug-drug interactions and interpatient variability in drug exposure. However, currently recommended practices can frequently fail to provide reliable estimates of fractional contributions to ($f_m$) of specific P450 enzymes to drug clearance. In this report, we describe a two-step qualitative-then-quantitative reaction phenotyping approach that yields more accurate estimates of $f_m$.**

## Introduction

Pharmacokinetic drug-drug interactions (DDI), wherein one drug (the "perpetrator" or "precipitant") alters the clearance of a second drug (the "victim" or "object"), is important in pharmacotherapy and new drug development. This can occur by a variety of mechanisms, but the most common is when an enzyme responsible for metabolism of a victim drug is inhibited or inactivated by a perpetrator drug. The potential magnitude of a DDI depends on the relative fractional contributions of individual enzymes to the metabolic clearance of the victim drug ($f_m$), as well as concentration and potency of the perpetrator drug, as described in the following equation (Rowland and Matin, 1973):

$$\mathrm{DDI} = \frac{1}{\left(\frac{f_m}{1+\left(\frac{[I]}{K_i}\right)}\right)+(1-f_m)} \quad (1)$$

Thus, the larger the value for $f_m$, the larger the potential DDI can be. This concept can be extended to pharmacogenetics to understand the potential magnitude of differences in exposure to a drug that is metabolized by a drug-metabolizing enzyme subject to genetic polymorphism. This simple concept can be further complicated by application of the extended clearance concept wherein drug transport processes can have an impact on overall clearance, and thus enhance or temper the magnitude of DDI caused by alterations in metabolism (Yoshida et al., 2013). Nevertheless, the concept of $f_m$ remains important.

In vitro methods to estimate the relative contributions, i.e., $f_m$ values, of specific human cytochrome P450 (P450) enzymes to the overall metabolism of drugs have been applied for over 30 years (Gelboin et al., 1985). The three main tools/approaches to conduct these experiments are 1) individually expressed P450 enzymes, 2) inhibitory antibodies and chemical inhibitors of defined selectivity, and 3) correlation to

This work received no external funding. Authors are employees and shareholders in Pfizer Inc.

No author has an actual or perceived conflict of interest with the contents of this article.

dx.doi.org/10.1124/dmd.122.000883.

S This article has supplemental material available at dmd.aspetjournals.org.

**ABBREVIATIONS:** DDI, drug-drug interaction; EMA, European Medicines Agency; $f_{CL}$, fraction of the total metabolism contributed by a metabolic pathway; $f_{CONTR}$, fraction of metabolic pathway contributed by an isoform; FDA, US Food and Drug Administration; $f_m$, fraction of metabolism; HPLC, high-performance liquid chromatography; HRMS, high-resolution mass spectrometry; ISEF, intersystem extrapolation factor; P450, cytochrome P450; PPP, 2-phenyl-2-(1-piperidinyl)propane; rP450, recombinant P450; TAO, troleandomycin; UHPLC, ultrahigh pressure liquid chromatography.

P450 marker activities measured in panels of liver microsome lots obtained from individual donors. These became available in the early 1990s and have evolved and improved since that time. Methods became defined by the late 1990s (Parkinson, 1996; Rodrigues, 1999) and were summarized in a cross-pharmaceutical industry position paper (Bjornsson et al., 2003). Despite common and widespread application, these methods suffer some limitations (Bohnert et al., 2016). The use of relative activity factors, relative abundance factors, and intersystem extrapolation factors (ISEFs) for scaling in vitro data gathered in individually expressed P450 enzymes can be confounded by substrate-dependent activity differences (Siu and Lai, 2017; Lindmark et al., 2018; Wang et al., 2019; Dantonio et al., 2022). Inhibitors commonly used as probes do not possess adequate selectivity to their target enzymes, and this can limit accuracy of $f_m$ (Lu et al., 2003; Khojasteh et al., 2011; Nirogi et al., 2015; Doran et al., 2022). Also, correlation analysis does not yield $f_m$ values, and can only be successful when the relative contribution by a P450 enzyme is high. These challenges are all compounded by the possibility of involvement of other non-P450 enzymes, which must also be defined in any given study to define $f_m$ values.

In this work, an alternate methodological approach to P450 reaction phenotyping has been defined. Instead of using two of the three aforementioned approaches in parallel as described in position papers and regulatory guidance documents [Bjornsson et al., 2003; Bohnert et al., 2016; US Food and Drug Administration (FDA), 2020; European Medicines Agency (EMA), 2012] and hoping for results of quantitative concurrence, a sequential qualitative-then-quantitative process (a.k.a., "mapping and detailing") is described that combines modern high-resolution mass spectrometry (HRMS) drug biotransformation experiments in individual P450 enzymes with more thorough chemical inhibition experiments and complex data fitting. In the first step, a drug of interest is incubated with a wide panel of individual P450 enzymes at a high concentration and metabolite profiles are determined using high-performance liquid chromatography UV–HRMS to identify, qualitatively, which P450 enzymes demonstrate any capability for generating metabolites. In the second step, metabolism of the drug of interest is measured quantitatively in pooled human liver microsomes in the presence and absence of inhibitors for P450 enzymes identified in the first step. The range of inhibitor concentrations and number of datapoints in the second step is high in order to delineate inhibition curves that can be reliably fit to complex functions and account for suboptimal inhibitor selectivity (Doran et al., 2022). This approach was evaluated using 48 drugs for step 1 and five of those (shown in Fig. 1) were selected to progress to step 2. Data were compared with clinical observations. This method is proposed as one that yields $f_m$ data of greater confidence and avoids spurious assignments of P450 enzymes that do not have meaningful contributions to the metabolism of individual drugs.

## Materials and Methods

**Materials.** Pooled human liver microsomes (50 donors, mixed sex) were prepared under contract by Xenotech (Lenexa, KS) and were stored in 20% glycerol at 20 mg/mL at −80°C. Individual heterologously expressed human P450 enzymes in the baculosome system, each at 1 nmol P450/mL, were obtained from Corning Life Sciences (Tewksbury, MA). Cryopreserved human hepatocytes were a custom mix of 13 donors of both sexes prepared under contract by BioIVT (Baltimore, MD). The 48 drugs used in this analysis were from either Sigma-Aldrich (St. Louis, MO) or Sequoia Research Products (Pangbourne, UK). Metabolites of escitalopram, fluvastatin, pioglitazone, risperidone, and propranolol used as standards for bioanalysis were prepared by biosynthesis using a previously described method (Walker, et al., 2014), with the exceptions of the following, which were purchased from commercial sources: N-desmethylcitalopram and 5-hydroxypropranolol (Toronto Research Chemicals; North York, Ontario, Canada); 9-hydroxyrisperidone (paliperidone, USP; North Bethesda, MD); and 4-hydroxypropranolol, N-desiospropylpropranolol; and 6-fluoro-3-(4-piperidinyl)-1,2-benzisoxazole (Sigma-Aldrich). NADPH (tetrasodium salt) was from Sigma-Aldrich. Williams E medium was from Thermo Fisher (Waltham, MA).

**Metabolite Profiles in Recombinant P450 Enzymes.** Drugs (10 μM) were incubated with 17 individually expressed P450 enzymes (100 pmol/mL) or human liver microsomes (2 mg/mL) and NADPH (1.3 mM) in 0.2 mL of potassium phosphate buffer (100 mM, pH 7.5) containing $MgCl_2$ (3.3 mM). The recombinant P450s (rP450s) evaluated were CYP1A1, CYP1A2, CYP1B1, CYP2A6, CYP2B6, CYP2C8, CYP2C9, CYP2C18, CYP2C19, CYP2D6, CYP2E1, CYP2J2, CYP3A4, CYP3A5, CYP3A7, CYP4A11, and CYP4F2, all wild type. Incubations were initiated with the addition of enzymes and conducted for 1 hour at 37°C in a shaking water bath. Incubations were terminated with the addition of acetonitrile (0.6 mL) and spun in a centrifuge at 1800*g* for 6 minutes. Supernatants (0.6 mL) were transferred to limited-volume glass inserts and subjected to vacuum centrifugation to remove the liquid. The residues were reconstituted in 0.1 mL 20% acetonitrile in water, spun at 1800*g* for 5 minutes for analysis by ultrahigh pressure liquid chromatography (UHPLC)–UV-HRMS.

The UHPLC-UV-HRMS system consisted of a Thermo Fisher Vanquish quaternary pumping system, with the autoinjector maintained at 10°C, column heater held at 45°C, and diode array UV detector operated at a wavelength range of 200–500 nm at 4 nm intervals at 50 Hz, in line with a Thermo Fisher Elite Orbitrap mass spectrometer. Separations were affected on a Phenomenex Kinetex XB-C18 column (2.3 × 100 mm; 2.6 μ) using one of two mobile phases—acidic or neutral—at a flow rate of 0.4 mL/min. The acidic mobile phase was 0.1% formic acid in water and acetonitrile and the neutral mobile phase was 10 mM ammonium acetate in water and acetonitrile. Mobile phase gradients were adjusted to optimize separations for each drug and its metabolites. The eluent was introduced into a heated electrospray ionization source on the mass spectrometer operated in the positive ion mode. Source settings were 4 kV for potential; 375°C and 275°C for source and capillary temperatures; and flows of 50, 20, and 2 for sheath, auxiliary, and sweep gas, respectively (arbitrary units). The orbitrap was set to scan a range of 100–1000 *m/z* at a resolution setting of 30000.

The data were interrogated first by visual inspection of the UV data using an extracted wavelength maximum for the parent drug and comparing data from P450-containing incubations to those in an incubation that contained

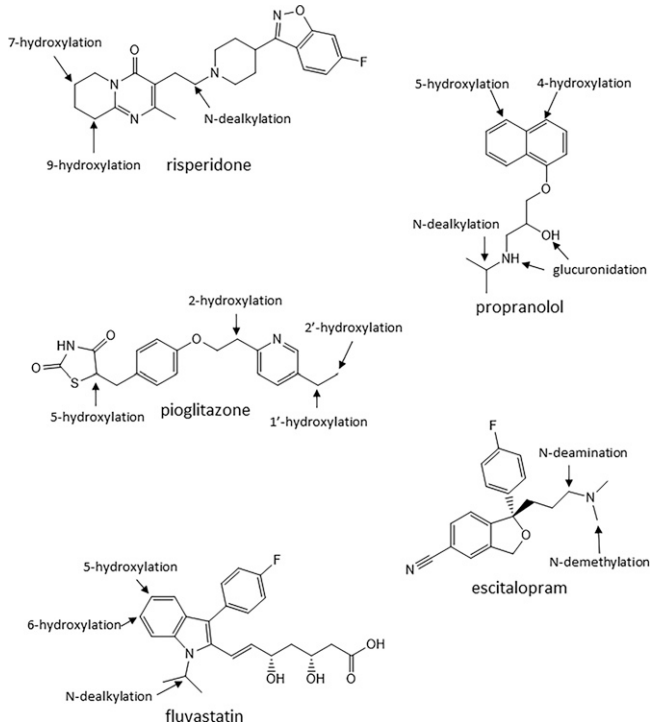


**Fig. 1.** Metabolism of escitalopram, fluvastatin, pioglitazone, propranolol, and risperidone.

microsomes from nontransfected control. They were then interrogated similarly by visual inspection of total ion current, and ultimately ion current of extracted ions of likely P450 biotransformation products (e.g., hydroxylation, heteroatom dealkylation, etc.) at a resolution of 5 ppm. A positive response was considered as a peak that had a height that was twice the background in the control incubation.

**Enzyme Kinetics in Human Liver Microsomes and Human Hepatocytes.** To select an appropriate sub-$K_M$ concentration for subsequent inhibition experiments, the enzyme kinetics for the metabolism of escitalopram, fluvastatin, pioglitazone, propranolol, and risperidone were determined in either pooled human liver microsomes or pooled human hepatocytes using previously determined time and optimized protein or cell density linear conditions. In general, for human liver microsome incubations, substrates were incubated in 100 mM potassium phosphate buffer (pH 7.4) containing $MgCl_2$ (3.3 mM) and NADPH (1.3 mM) at 37°C. Incubations were terminated with the addition of acetonitrile containing internal standard. In general, for human hepatocyte incubations, substrates were incubated in a custom formula of William's E Medium supplemented with 26 mM $NaHCO_3$ in an incubator set to 37°C with 5% $CO_2$ and 75% relative humidity. Incubations were commenced with the addition of substrate and terminated with the addition of acetonitrile containing internal standard. Details of the incubation conditions for each of the five substrates are listed in Supplemental Tables 1–3, and the bioanalytical methods used for each are listed in Supplemental Tables 4 and 5. Experiments were run in triplicate. Enzyme kinetic parameters were determined as described below.

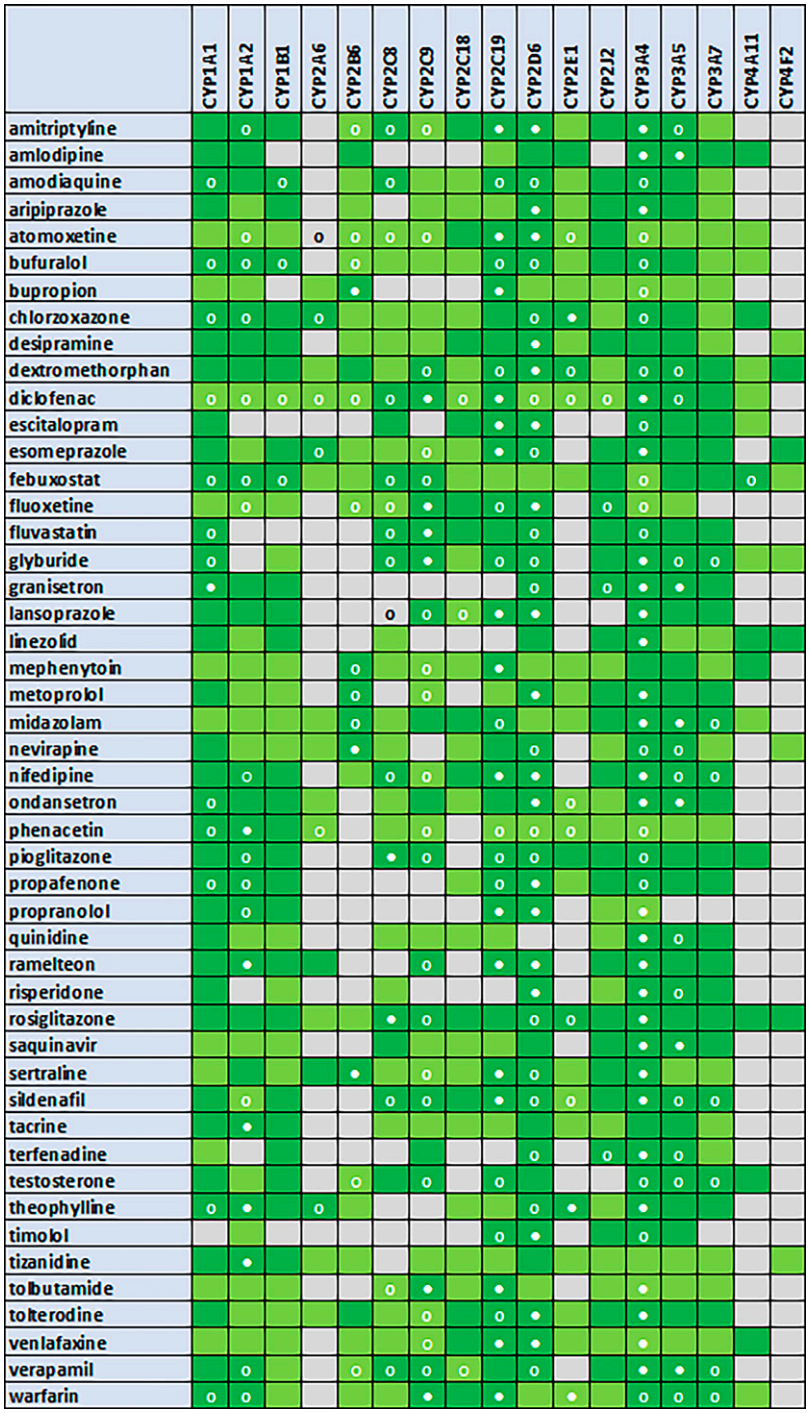


**Fig. 2.** Summary of metabolism of 48 drugs by 17 rCYP enzymes. Dark green boxes indicate the observation of metabolites by HPLC-UV and mass spectrometry. Pale green boxes indicate the observation of metabolites only by mass spectrometry. Gray boxes indicate that no metabolism was observed. The presence of a solid circle indicates that there is clinical and in vitro evidence for the involvement of an enzyme in the metabolism of the drug, while an open circle indicates that there is only in vitro evidence for the involvement of an enzyme in the metabolism of the drug. A list of the literature references supporting the placement of solid and open circles is in the Supplemental Information.

TABLE 1

Enzyme kinetics and calculated $f_{CL}$ values for the metabolism of escitalopram, fluvastatin, pioglitazone, propranolol, and risperidone.

*Values for $V_{max}$ and $K_M$ are mean (S.E.). Velocity units are in pmol/min/mg microsomal protein for fluvastatin, pioglitazone, and risperidone. Units are in pmol/min/million cells for escitalopram and propranolol. Intrinsic clearance units are μL/min/mg for fluvastatin, pioglitazone, and risperidone and μL/min/million cells for escitalopram and propranolol. Units for KM are in uM.*

| Drug/Reaction | $V_{max}$ (1) | $K_M$ (1) | $CL_{int}$ (1) | $V_{max}$ (2) | $K_M$ (2) | $CL_{int}$ (2) | Total $CL_{int}$ | Pathway $f_{CL}$ |
|---|---|---|---|---|---|---|---|---|
| Escitalopram[a] | | | | | | | | |
| N-demethylation | 30.6 (2.34) | 46.9 (6.63) | 0.652 | — | — | — | 0.652 | 0.80 |
| N-deamination | 12.1 (0.82) | 76.2 (9.63) | 0.159 | — | — | — | 0.159 | 0.20 |
| Fluvastatin | | | | | | | | |
| 5-hydroxylation | 6.53 (0.26) | 0.326 (0.026) | 20.0 | 4.11 (0.22) | 11.6 (2.3) | 0.35 | 20.4 | 0.36 |
| 6-hydroxylation | 499 (5) | 20.9 (0.5) | 23.9 | — | — | — | 23.9 | 0.42 |
| N-dealkylation | 3.76 (0.08) | 0.318 (0.015) | 11.8 | 4.61 (0.07) | 18.1 (1.3) | 0.26 | 12.1 | 0.21 |
| Pioglitazone[b] | | | | | | | | |
| 1'-hydroxylation | 214 (10.2) | 9.22 (0.8) | 23.2 | — | — | — | 23.2 | 0.45 |
| 2-hydroxylation | 29.6 (1.0) | 4.90 (0.3) | 6.05 | — | — | — | 6.05 | 0.12 |
| 2'-hydroxylation | 26.3 (1.1) | 1.83 (0.2) | 14.4 | — | — | — | 14.4 | 0.28 |
| 5-hydroxylation | 484 (37) | 61.6 (5.9) | 7.85 | — | — | — | 7.85 | 0.15 |
| Propranolol[a] | | | | | | | | |
| Glucuronidation 1 | 30.6 (10.3) | 15.2 (5.3) | 2.01 | 47.6 (5.5) | 177 (114) | 0.269 | 2.28 | 0.075 |
| Glucuronidation 2 | 33.9 (15.5) | 13.0 (5.5) | 2.61 | 35.3 (11.7) | 106 (90) | 0.333 | 2.94 | 0.097 |
| 4-hydroxylation | 33.9 (1.2) | 1.46 (0.10) | 22.6 | 35.6 (2.0) | 113 (25) | 0.315 | 22.9 | 0.77 |
| 5-hydroxylation | 0.57 (0.1) | 5.06 (1.08) | 0.113 | — | — | 0.013 | 0.126 | 0.004 |
| N-dealkylation | 16.0 (2.4) | 11.7 (3.0) | 1.37 | — | — | 0.176 | 1.55 | 0.051 |
| Risperidone | | | | | | | | |
| 7-hydroxylation | 16.2 (1.4) | 10.5 (2.3) | 1.54 | — | — | 0.063 (0.005) | 1.61 | 0.16 |
| 9-hydroxylation | 170 (23) | 27.3 (7.2) | 6.23 | — | — | 0.59 (0.07) | 6.82 | 0.67 |
| N-dealkylation | 92.1 (4.1) | 57.5 (3.7) | 1.60 | — | — | 0.14 (0.01) | 1.74 | 0.17 |

[a]Data for escitalopram and propranolol are from pooled human hepatocytes.
[b]Pioglitazone enzyme kinetics best fit a model that also included substrate inhibition with $K_s$ values of 65.4, 67.2, 76.5, and 23.5 μM for 1', 2, 2', and 5-hydroxylation pathways, respectively.

**Inhibition of P450 Activity in Human Liver Microsomes.** Inhibition experiments were conducted using the same incubation conditions listed for each substrate in Supplemental Tables 1 and 2. Fixed substrate concentrations were used: escitalopram (4 μM), fluvastatin (0.1 μM), pioglitazone (0.3 μM), propranolol (0.5 μM), and risperidone (1.0 μM). P450-selective inhibitors were evaluated at both single concentrations and >18-point concentration curves. The concentration ranges used for each were: furafylline for CYP1A2 (0.01–20 μM or 100 μM), phenylethylpiperidine (PPP) for

TABLE 2

Single-inhibitor concentration data for the metabolism of escitalopram, fluvastatin, pioglitazone, propranolol, and risperidone and estimates of $f_m$.

*Percent inhibition data are mean (S.E.); values labeled with an asterisk (*) are statistically significant. Estimated $f_m$ calculated only from enzymes with statistically significant outcomes. The single concentrations of inhibitors used for these estimates are listed in Supplemental Table 9.*

| | $f_{CL}$ | CYP1A2 | CYP2B6 | CYP2C8 | CYP2C9 | CYP2C19 | CYP2D6 | CYP3A | Sum |
|---|---|---|---|---|---|---|---|---|---|
| Escitalopram | | | | | | | | | |
| N-demethylation | 0.80 | 7.3 (5.7) | 15.6 (3.7)* | 34.2 (2.5)* | 6.7 (10.0) | 31.3 (1.6)*[a] | 10.3 (6.5) | 43.3 (2.5)* | |
| N-deamination | 0.20 | ND[c] | ND[c] | ND[c] | ND[c] | 89.0 (1.4)*[a] | ND[c] | ND[c] | |
| Estimated $f_m$ | | | 0.13 | 0.28 | | 0.43 | | 0.35 | 1.19 |
| Fluvastatin | | | | | | | | | |
| 5-hydroxylation | 0.36 | <0[b] | <0[b] | <0[b] | 95.0 (0.4)* | 11.9 (1.4)* | 3.7 (3.9) | 23.9 (2.3)* | |
| 6-hydroxylation | 0.42 | <0[b] | <0[b] | 0.5 (6.9) | 61.2 (1.4)* | 10.5 (2.6)* | <0[b] | 31.5 (1.4)* | |
| N-dealkylation | 0.21 | <0[b] | <0[b] | <0[b] | 96.6 (1.4)* | 10.2 (2.6)* | 2.8 (2.6) | 9.8 (1.3)* | |
| Estimated $f_m$ | | | | | 0.81 | 0.11 | | 0.24 | 1.16 |
| Pioglitazone | | | | | | | | | |
| 1'-hydroxylation | 0.45 | <0[b] | 1.2 (1.4) | 76.3 (4.0)* | <0[b] | <0[b] | <0[b] | <0[b] | |
| 2-hydroxylation | 0.12 | <0[b] | 0.4 (4.1) | 52.4 (4.3)* | 31.5 (6.4)* | <0[b] | <0[b] | <0[b] | |
| 2'-hydroxylation | 0.28 | <0[b] | <0[b] | 69.1 (5.3)* | <0[b] | <0[b] | <0[b] | <0[b] | |
| 5-hydroxylation | 0.15 | 29.2 (5.8)* | 2.3 (6.3) | 4.5 (13.2) | 5.4 (9.1) | <0[b] | <0[b] | 24.3 (1.9)* | |
| Estimated $f_m$ | | 0.04 | | 0.60 | 0.04 | | | 0.04 | 0.72 |
| Propranolol[d] | | | | | | | | | |
| 4-hydroxylation | 0.77 | 0.6 (14.9) | 11.7 (10.0) | 19.0 (9.7) | 3.5 (6.4) | 1.1 (8.8) | 91.1 (11.6)* | 0.93 (4.5) | |
| 5-hydroxylation | 0.004 | <0[b] | 16.4 (17.7) | 24.4 (17.0) | 11.4 (9.9) | 11.9 (12.6) | 88.5 (10.2)* | <0[b] | |
| N-dealkylation | 0.05 | 70.2 (5.0)* | 3.3 (10.5) | 28.0 (7.9) | 23.3 (8.7) | 16.7 (8.8) | 35.3 (7.3)* | 0.56 (2.1) | |
| Estimated $f_m$ | | 0.04 | | | | | 0.73 | | 0.77 |
| Risperidone | | | | | | | | | |
| 7-hydroxylation | 0.16 | <0[b] | 12.9 (7.3) | 22.2 (5.5)* | 12.9 (7.3) | <0[b] | 87.4 (2.3)* | <0[b] | |
| 9-hydroxylation | 0.67 | <0[b] | 13.4 (14.5) | 23.2 (5.3) | 16.8 (11.6) | 7.4 (7.3) | 62.4 (4.2)* | 25.8 (1.6)* | |
| N-dealkylation | 0.17 | <0[b] | 39.2 (17.1) | 30.8 (7.0) | 39.2 (17.1) | 24.0 (6.8)* | 19.7 (8.1) | 90.4 (7.9)* | |
| Estimated $f_m$ | | | | 0.04 | | 0.04 | 0.56 | 0.33 | 0.97 |

[a]Data for CYP2C19 catalyzed escitalopram metabolism were from esomeprazole in human hepatocytes.
[b]Rates in inhibited incubation were greater than in the control incubation.
[c]ND, not determined.
[d]$f_{CL}$ excludes the contribution of glucuronidation determined in human hepatocyte kinetics reported in Table 1.

CYP2B6 (0.01–100 μM), montelukast for CYP2C8 (0.001–10 μM), sulfaphenazole for CYP2C9 (0.01–100 μM), N-benzylnirvanol for CYP2C19 (0.005–50 μM), quinidine for CYP2D6 (0.0001–10 μM), and troleandomycin for CYP3A (0.01–100 μM). Since furafylline, troleandomycin (TAO), and PPP are time-dependent inhibitors, these were each preincubated for 10 minutes with microsomes and NADPH prior to addition of substrate. Positive control substrate reactions for each inhibitor were included using a previously established method (Supplemental Tables 6 and 7) and nonspecific binding of the inhibitors to microsomes was corrected based on previously determined values (Supplemental Table 8; Doran et al., 2022).

The percent activity remaining was obtained by normalizing metabolite concentration data to the averaged solvent controls. The inhibitory profiles were generated using GraphPad Prism for Windows (version 9). In general, nonlinear regression of the data were conducted using the log [I] versus normalized response with variable slope model to better fit the data, which uses the following inhibitory equation (referred to as the "four-parameter fit"):

$$Y = \text{Bottom} + \frac{\text{Top} - \text{Bottom}}{1 + e^{h(\ln x - \ln IC_{50})}} \quad (2)$$

where $Y$ is the percent of control activity remaining and $x$ is the inhibitor concentration. The four parameters in the model are the $IC^{50}$, which represents the inhibitor concentration that yields a response halfway between the upper and lower asymptotes; the hill slope (h), which represents the steepness of the curve; and the upper and lower asymptotes (Top and Bottom, respectively), which represent the maximum and minimum possible responses. The maximal contribution of a P450 was determined by the span or the difference between the fitted upper and lower asymptotes:

$$\text{span} = \text{Top} - \text{Bottom} \quad (3)$$

In certain instances, the above equation was not able to fit the data, and the equation below was used to fit the data (referred to as the "six-parameter fit"):

$$Y = I_{max} - MAX_A + \left(\frac{MAX_A}{1 + e^{h(\ln x - \ln IC_{50}A)}}\right) - MAX_B + \left(\frac{MAX_B}{1 + e^{h(\ln x - \ln IC_{50}B)}}\right) \quad (4)$$

where $Y$ is the percent control activity remaining and $x$ is the inhibitor concentration. The six parameters in the model are $MAX_A$ and $MAX_B$, which represent the maximum contribution of enzymes A and B, respectively; $IC_{50A}$ and $IC_{50B}$, which are the inflection points for the inhibitor on enzymes A and B, respectively; the hill slope (h), which represents the steepness of the curve for enzymes A and B; and $I_{max}$, which represents the maximum possible response (Doran et al., 2022).

**Rates of Metabolism in rP450 Enzymes.** The metabolism of the five drugs was measured in seven major hepatically expressed rCYP enzymes. Specifics for each drug are listed in Supplemental Table 3. In general, each drug was incubated with 1, 10, and 100 pmol P450/mL in 100 mM potassium phosphate buffer containing $MgCl_2$ (3.3 mM) and NADPH (1.3 mM). Incubations were commenced with the addition of NADPH and carried out at 37°C. At various times up to 60 minutes, aliquots were removed and reactions terminated by addition to four volumes of acetonitrile containing internal standard. Substrate concentrations were below $K_M$ values that had been determined in either human liver microsomes or human hepatocytes. Reaction velocities were determined from the product formed versus time plots at the incubation condition that yielded linear product formation over the longest incubation time and at the lowest enzyme concentration.

**Estimation of $f_m$ Values.** Estimations of $f_m$ values were made as follows. Enzyme kinetic data were used to calculate intrinsic clearance ($CL_{int}$) for each metabolic pathway in pooled human liver microsomes:

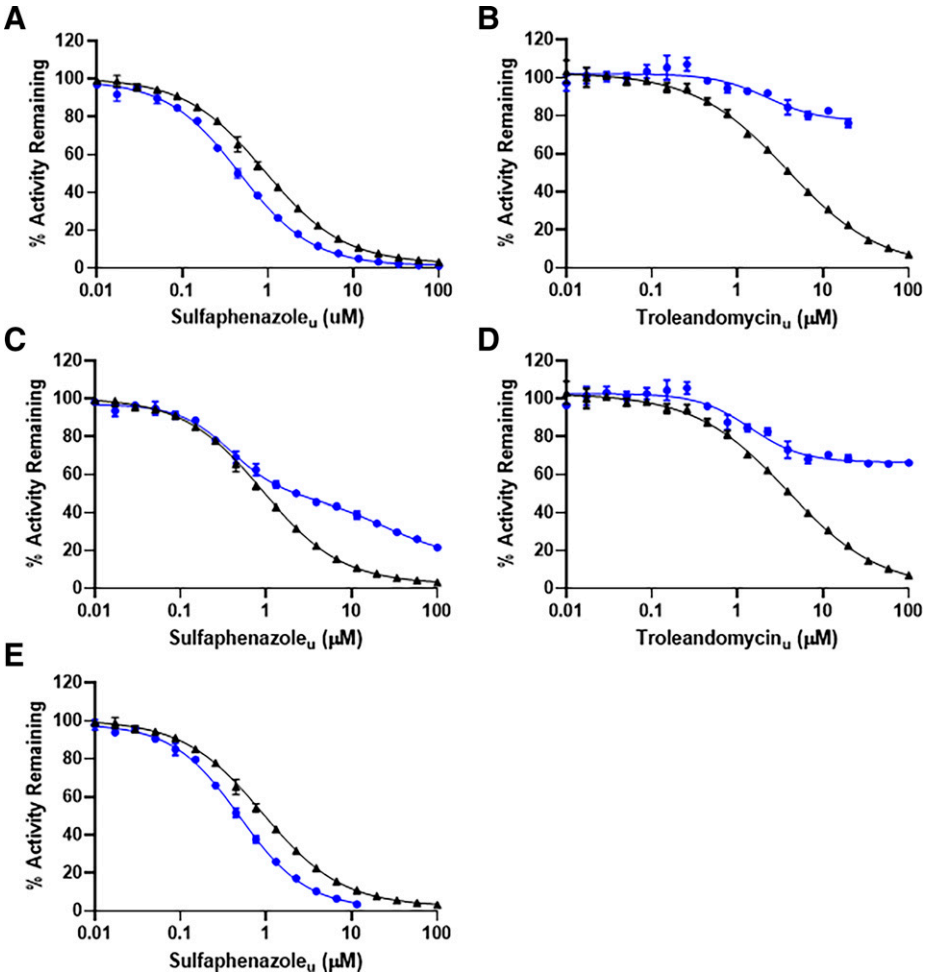


**Fig. 3.** Inhibition curves for metabolism of fluvastatin. (A and B) Effect of sulfaphenazole and troleandomycin on 5-hydroxylation. (C and D) Effect of sulfaphenazole and troleandomycin on 6-hydroxlation. (E) Effect of sulfaphenazole on N-dealkylation. Blue curves represent fluvastatin metabolism and black curves represent the positive control reactions for CYP2C9 (diclofenac 4'-hydroxylation) and CYP3A (midazolam 1'-hydroxylation).

TABLE 3

Maximum percentage inhibition values ($MAX_A$) from multiple concentration inhibition experiments for the metabolism of escitalopram, fluvastatin, pioglitazone, propranolol, and risperidone and estimates of $f_m$.

*Maximum percentage inhibition data are mean (SE). All unbound $IC_{50}$ values are listed in Supplemental Table 11.*

| | Pathway $f_{CL}$[a] | Enzyme | | | | | | | Sum $f_m$ |
|---|---|---|---|---|---|---|---|---|---|
| | | CYP1A2 | CYP2B6 | CYP2C8 | CYP2C9 | CYP2C19 | CYP2D6 | CYP3A | |
| Escitalopram | | | | | | | | | |
| N-demethylation | 0.80 | — | — | 24.3 (7.1) | — | 28.3 (1.7)[b] | 19.5 (2.01) | 36.0 (3.1) | |
| N-deamination | 0.20 | — | — | — | — | 97.1 (5.2)[b] | — | — | |
| Estimated $f_m$ | | — | — | 0.20 | — | 0.42 | 0.16 | 0.29 | 1.07 |
| Fluvastatin | | | | | | | | | |
| 5-hydroxylation | 0.36 | — | — | — | 98.0 (0.9) | — | — | — | |
| 6-hydroxylation | 0.42 | — | — | — | 47.7 (2.7) | — | — | 36.3 (1.7) | |
| N-dealkylation | 0.21 | — | — | — | 97.2 (1.5) | — | — | — | |
| Estimated $f_m$ | | — | — | — | 0.77 | — | — | 0.15 | 0.92 |
| Pioglitazone | | | | | | | | | |
| 1'-hydroxylation | 0.45 | — | — | 85.1 (2.2) | — | — | — | — | |
| 2-hydroxylation | 0.12 | — | — | 44.9 (7.6) | 31.4 (2.7) | — | — | — | |
| 2'-hydroxylation | 0.28 | — | — | 100 (5.8) | — | — | — | — | |
| 5-hydroxylation | 0.15 | — | — | — | — | — | — | 32.8 (2.4) | |
| Estimated $f_m$ | | — | — | 0.72 | 0.04 | — | — | 0.05 | 0.81 |
| Propranolol[c] | | | | | | | | | |
| 4-hydroxylation | 0.77 | — | — | — | — | — | 86.0 (3.5) | — | |
| 5-hydroxylation | 0.004 | — | — | — | — | — | 76.1 (2.8) | — | |
| N-dealkylation | 0.05 | 68.9 (4.8) | 33.6 (6.0) | — | — | — | 17.5 (2.0) | — | |
| Estimated $f_m$ | | 0.03 | 0.02 | — | — | — | 0.68 | — | 0.73 |
| Risperidone | | | | | | | | | |
| 7-hydroxylation | 0.16 | — | — | — | — | — | 91.4 (2.9) | — | |
| 9-hydroxylation | 0.67 | — | — | — | — | — | 67.1 (4.1) | 24.9 (2.7) | |
| N-dealkylation | 0.17 | — | — | — | — | — | — | 99.1 (7.1) | |
| Estimated $f_m$ | | — | — | — | — | — | 0.60 | 0.34 | 0.94 |

[a]Human hepatocyte-derived $f_{CL}$ values for escitalopram and propranolol, all others in human liver microsomes.
[b]From chemical inhibition conducted in human hepatocytes.
[c]$f_{CL}$ excludes the contribution of UGT metabolism determined in human hepatocyte kinetics reported in Table 1.

$$CL_{int,\,pathwayX} = \frac{V_{max}}{K_M}(\text{one} - \text{enzyme model}) \quad (5)$$

or

$$CL_{int,\,pathwayX} = \frac{V_{max(1)}}{K_{M(1)}} + CL_{int(2)}(\text{two} - \text{enzyme model}) \quad (6)$$

in which $CL_{int,pathwayX}$ refers to the intrinsic clearance for a specific metabolic pathway, $V_{max}$ and $K_M$ are the maximum reaction velocity and Michaelis constant for that pathway, and, when necessary, $CL_{int(2)}$ represents a high capacity/high $K_M$ enzyme activity wherein the $K_M$ was greater than the highest substrate concentration evaluated.

TABLE 4

ISEF adjusted rCYP rate data for escitalopram, fluvastatin, pioglitazone, propranolol, and risperidone.

*Rate data are expressed in intrinsic clearance terms (v/[S]) and are in units of μL/min/mg microsomes. Values represent the measured rates from Supplemental Table 10 multiplied by the P450-specific ISEF and P450 abundance in human liver microsomes.*

| | CYP1A2 | CYP2B6 | CYP2C8 | CYP2C9 | CYP2C19 | CYP2D6 | CYP3A4 |
|---|---|---|---|---|---|---|---|
| ISEF | 0.052 | 1.3 | 1.8 | 0.38 | 0.33 | 0.054 | 0.19 |
| P450 abundance[a] | 52 | 17 | 24 | 73 | 14 | 8 | 137 |
| Escitalopram | | | | | | | |
| N-demethylation | 0.00124 | — | 1.60 | — | 0.246 | 3.44 | 0.567 |
| N-deamination | — | — | — | — | 0.016 | — | — |
| Fluvastatin | | | | | | | |
| 5-hydroxylation | — | — | — | 6.57 | — | — | — |
| 6-hydroxylation | — | — | 2.85 | 5.27 | — | 0.016 | 16.8 |
| N-dealkylation | — | — | — | 0.591 | — | — | — |
| Pioglitazone | | | | | | | |
| 1'-hydroxylation | 0.133 | — | 10.3 | 0.407 | 0.083 | 0.024 | 0.097 |
| 2-hydroxylation | — | — | 1.09 | 0.366 | — | — | – |
| 2'-hydroxylation | — | — | 1.88 | — | — | — | – |
| 5-hydroxylation | — | — | 0.209 | — | — | — | 0.802 |
| Propranolol | | | | | | | |
| 4-hydroxylation | 1.60 | 0.00171 | 0.0619 | 0.00566 | 0.00444 | 7.15 | 1.44 |
| 5-hydroxylation | 0.340 | — | 0.00753 | 0.00971 | — | 0.630 | 0.0256 |
| N-dealkylation | 3.16 | 0.0544 | 0.0243 | 0.0189 | 0.635 | 0.753 | 0.118 |
| Risperidone | | | | | | | |
| 7-hydroxylation | — | — | 0.0372 | — | 0.00517 | 0.0791 | 0.0113 |
| 9-hydroxylation | — | — | 0.165 | — | 0.0223 | 0.566 | 3.28 |
| N-dealkylation | — | — | — | — | — | — | 19.9 |

[a]Units of pmol P450/mg human liver microsomal protein.

TABLE 5

Percent contribution and $f_m$ values estimated from rCYP rate data for escitalopram, fluvastatin, pioglitazone, propranolol, and risperidone.

*Individual metabolic pathway enzyme $f_m$ values represent the ISEF-adjusted rates for each enzyme divided by the sum of rates across all enzymes (Table 4). $f_{CL}$ derived from enzyme kinetic parameters (Table 1). Final $f_m$ values for each enzyme are sums of the products of individual pathway $f_m$ values and $f_{CL}$ values.*

| | | Isoform Contribution by Pathway (Percent) | | | | | | |
|---|---|---|---|---|---|---|---|---|
| | Pathway $f_{CL}$[a] | CYP1A2 | CYP2B6 | CYP2C8 | CYP2C9 | CYP2C19 | CYP2D6 | CYP3A4 |
| Escitalopram | | | | | | | | |
| N-demethylation | 0.80 | 0.021 | — | 27.3 | — | 4.21 | 58.8 | 9.68 |
| N-deamination | 0.20 | — | — | — | — | 100 | — | — |
| Total enzyme $f_m$ | | <0.01 | | 0.22 | | 0.23 | 0.47 | 0.08 |
| Fluvastatin | | | | | | | | |
| 5-hydroxylation | 0.36 | — | — | — | 100 | — | — | — |
| 6-hydroxylation | 0.42 | — | — | 11 | 21 | — | 0.065 | 67 |
| N-dealkylation | 0.21 | — | — | — | 100 | — | — | — |
| Total enzyme $f_m$ | | | | 0.05 | 0.67 | | < 0.01 | 0.29 |
| Pioglitazone | | | | | | | | |
| 1'-hydroxylation | 0.45 | 1.2 | — | 93 | 3.7 | 0.76 | 0.22 | 0.88 |
| 2-hydroxylation | 0.12 | — | — | 75 | 25 | — | — | — |
| 2'-hydroxylation | 0.28 | — | — | 100 | — | — | — | — |
| 5-hydroxylation | 0.15 | — | — | 21 | — | — | — | 79 |
| Total Enzyme $f_m$ | | <0.01 | | 0.82 | 0.05 | <0.01 | <0.01 | 0.13 |
| Propranolol[b] | | | | | | | | |
| 4-hydroxylation | 0.77 | 16 | 0.017 | 0.60 | 0.055 | 0.043 | 70 | 14 |
| 5-hydroxylation | 0.004 | 34 | — | 0.74 | 1.0 | — | 62 | 2.5 |
| N-dealkylation | 0.05 | 66 | 1.1 | 0.51 | 0.40 | 13 | 16 | 2.5 |
| Total enzyme $f_m$ | | 0.16 | <0.01 | <0.01 | <0.01 | <0.01 | 0.55 | 0.11 |
| Risperidone | | | | | | | | |
| 7-hydroxylation | 0.16 | — | — | 2.8 | — | 3.9 | 60 | 8.6 |
| 9-hydroxylation | 0.67 | — | — | 4.1 | — | 0.55 | 14 | 81 |
| N-dealkylation | 0.17 | — | — | — | — | — | — | 100 |
| Total enzyme $f_m$ | | | | 0.07 | | 0.01 | 0.19 | 0.73 |

[a]Human hepatocyte-derived $f_{CL}$ values for escitalopram and propranolol, all others in human liver microsomes.
[b]$f_{CL}$ excludes the contribution of UGT metabolism determined in HHEP kinetics reported in Table 1.

These $CL_{int}$ values were used to calculate the fraction of metabolic clearance proceeding through a pathway ($f_{CL}$) by dividing the $CL_{int}$ for the pathway of interest by the sum of $CL_{int}$ values of all pathways:

$$f_{CL,pathwayX} = \frac{CL_{int,pathwayX}}{\mathrm{CL_{int,\,all\ \ pathways}}} \tag{7}$$

The fractional clearance values for each pathway were scaled to the respective isoform contributions to determine the fraction metabolized using the following general equation:

$$\mathrm{f_{m,\,CYPA}} = (\mathrm{f_{CL,\,pathwayX}} \cdot \mathrm{f_{CONTR,\,CYPA,\,pathwayX}}) + (\mathrm{f_{CL,\,pathwayY}} \cdot \mathrm{f_{CONTR,\,CYPA,\,pathwayY}}) + (\mathrm{f_{CL,\,pathwayZ}} \cdot \mathrm{f_{CONTR,\,CYPA,\,pathwayZ}}) \tag{8}$$

where the term $f_{CONTR,CYPA,pathwayX}$ refers to the inhibition of metabolic pathway X in human liver microsomes by an inhibitor selective for CYPA. This was calculated in two ways:

For single-concentration inhibition experiments:

$$\mathrm{f_{CONTR,\,CYPA,\,pathwayX}} = \frac{\%\ \mathrm{inhibition_{CYPA,\,pathwayX}}}{100} \tag{9}$$

or for multiple-point inhibition experiments:

$$\mathrm{f_{CONTR,\,CYPA,\,pathwayX}} = \frac{\mathrm{span_{CYPA,\,pathwayX}}}{100} \tag{10}$$

$$\mathrm{f_{CONTR,\,CYPA,\,pathwayX}} = \frac{MAX_{\mathrm{A,\,CYPA,\,pathwayX}}}{100} \tag{11}$$

for the four-parameter and six-parameter inhibition models, respectively.

For data from heterologously expressed P450 enzymes, $f_m$ values were calculated as follows. Reaction velocities for each metabolic pathway for each P450 enzyme were divided by the substrate concentration evaluated in the assay to yield v/[S] values in units of μL/min/pmol P450. These values were converted to estimated values for each P450 enzyme in each metabolic pathway in pooled human liver microsomes:

$$\left(\frac{v}{[S]}\right)_{CYPA,\,pathwayX,\,HLM} = \left(\frac{v}{[S]}\right)_{CYPA,\,pathwayX} \cdot ISEF_{CYPA} \cdot \frac{pmoles\ \ of\ \ CYPA}{mg\ \ microsomal\ \ protein} \tag{12}$$

The ISEF values were determined from marker substrate activities and were 0.052, 1.30, 1.80, 0.38, 0.33, 0.054, and 0.19 for CYP1A2, CYP2B6, CYP2C8, CYP2C9, CYP2C19, CYP2D6, and CYP3A4, respectively. The values for abundance of each P450 enzyme in liver microsomes were 52, 17, 24, 73, 14, 8, and 137 pmol P450/mg protein for CYP1A2, CYP2B6, CYP2C8, CYP2C9, CYP2C19, CYP2D6, and CYP3A4, respectively. The $f_m$ values for each P450 on an individual metabolic pathway were determined as:

$$\mathrm{f_{m,\,CYPA,\,pathwayX}} = \frac{\left(\frac{v}{[S]}\right)_{\mathrm{CYPA,\,pathwayX,\,HLM}}}{\sum\left(\frac{v}{[S]}\right)_{\mathrm{all\ \ CYP,\,pathwayX,\,HLM}}} \tag{13}$$

The contribution of a specific P450 enzyme to the total metabolism was calculated as:

$$\mathrm{f_{m,\,CYPA}} = \mathrm{f_{m,\,CYPA,\,pathwayX}} + \mathrm{f_{m,\,CYPA,\,pathwayY}} + \mathrm{f_{m,\,CYPA,\,pathwayZ}} \tag{14}$$

**Statistical Treatment of Data.** For enzyme kinetic parameter determination, data were first plotted on Eadie-Hofstee plots for potential model assignment and then the v versus v/[S] data were fit in GraphPad Prism for Windows (version 9) to various models with selection of a model other than Michaelis-Menten based on the Akaike Information Criterion (Nagar et al., 2014). Single-point inhibition data were evaluated using Welch's unpaired two-sample *t* test with unequal variances and a significance threshold of 0.05 as described elsewhere (Doran et al., 2022). Full curve dose-response inhibition data from test compounds were fit using either the four-parameter, single $IC_{50}$ dose-response model or the six-parameter, double $IC_{50}$ dose-response model, using an extra

TABLE 6

Summary comparison of in vitro $f_m$ data for escitalopram, fluvastatin, pioglitazone, propranolol, and risperidone to in vivo $f_m$ values estimated from DDI or pharmacogenetic data.

| | | Estimate of $f_m$ From: | | | | | |
|---|---|---|---|---|---|---|---|
| Drug | Enzyme | rP450s and ISEF | Single Point Inhibition | Inhibition Curves | In Vivo | PGX or DDI | In Vivo References |
| Escitalopram | CYP2B6 | — | 0.13 | — | ND | | |
| | CYP2C8 | 0.22 | 0.28 | 0.20 | ND | | |
| | CYP2C19 | 0.23 | 0.43 | 0.42 | 0.36 | PGX | Herrlin et al., 2003; |
| | | | | | 0.45 | | Rudberg et al., 2009; |
| | | | | | 0.82 | | Rudberg et al., 2008; |
| | | | | | 0.72 | | Waade et al., 2014; |
| | | | | | 0.69 | | Jukić et al., 2018; |
| | | | | | 0.43 | | Tsuchimine et al., 2018 |
| | CYP2D6 | 0.47 | — | 0.16 | <0.01 | PGX | Herrlin et al., 2003 |
| | CYP3A4 | 0.08 | 0.35 | 0.29 | 0.08 | DDI | Gutierrez et al., 2003 |
| Fluvastatin | CYP2C8 | 0.05 | — | — | 0.06 | DDI | Spence et al., 1995 |
| | CYP2C9 | 0.67 | 0.81 | 0.76 | 0.76 | PGX | Kirchheiner et al., 2003 |
| | CYP2C19 | — | 0.11 | — | ND | | |
| | CYP2D6 | <0.01 | — | — | ND | | |
| | CYP3A4 | 0.29 | 0.24 | 0.15 | 0.12 | DDI | Kivisto et al., 1998 |
| Pioglitazone | CYP1A2 | — | 0.04 | — | ND | | |
| | CYP2C8 | 0.82 | 0.60 | 0.72 | 0.73 | DDI | Aquilante et al., 2013 |
| | CYP2C9 | 0.05 | 0.04 | 0.04 | ND | | |
| | CYP3A4 | 0.13 | 0.04 | 0.05 | 0.08 | DDI | Jaakkola et al., 2005 |
| Propranolol[a] | CYP1A2 | 0.16 | 0.04 | 0.03 | ND | | Byrne et al., 1984; |
| | | | | | | | McLean et al., 1980 |
| | CYP2B6 | <0.01 | — | 0.02 | ND | | |
| | CYP2C8 | <0.01 | — | — | ND | | |
| | CYP2C9 | <0.01 | — | — | ND | | |
| | CYP2C19 | <0.01 | — | — | 0.25 | PGX | Ward et al., 1989 |
| | CYP2D6 | 0.55 | 0.72 | 0.68 | 0.00 | PGX | Lennard et al., 1984 |
| | | | | | 0.37 | | Raghuram et al., 1984 |
| | | | | | 0.55 | DDI | Zhou et al., 1990 |
| | | | | | 0.56 | | Yasuhara et al., 1990 |
| | CYP3A4 | 0.11 | — | — | 0.39 | DDI | McCourty et al., 1988 |
| | | | | | 0.33 | | Tateishi et al., 1992 |
| | | | | | 0.32 | | Tateishi et al., 1989 |
| | | | | | 0.17 | | Dimmitt et al., 1991 |
| Risperidone | CYP2C8 | 0.07 | 0.04 | — | ND | | |
| | CYP2C19 | 0.01 | 0.04 | — | ND | | |
| | CYP2D6 | 0.19 | 0.56 | 0.60 | 0.66 | PGX | Gasso et al., 2014 |
| | | | | | 0.88 | | Cabaleiro et al., 2014 |
| | CYP3A4 | 0.73 | 0.32 | 0.34 | 0.36 | DDI | Mahatthanatrakul et al., 2012 |

ND, no in vivo data reported for these enzymes; PGX, pharmacogenetic data.
[a]$f_{CL}$ excludes the contribution of UGT metabolism determined in HHEP kinetics reported in Table 1.

sum-of-squares F-test to select the model that best fit the data. After fitting the dose-response curves to the test compound data, a two-one-sided *t* test equivalence procedure was used to determine if the $IC_{50}$ for the test compound was significantly within fivefold of the $IC_{50}$ for the probe substrate (Doran et al., 2022). When the six-parameter model was selected, the $IC_{50}$ of the first phase ($IC_{50A}$) of the curve was compared with the $IC_{50}$ of the probe substrate. If significant fivefold equivalence in $IC_{50}$ values between the test compound and probe was established, the reduction in percent activity of the test compound was compared with zero. For the four-parameter model, the span parameter (difference between upper asymptote and lower asymptote) needed to be significantly greater than zero, while the $MAX_A$ parameter needed to be significantly greater than zero for the six-parameter model. If both the equivalence test passed and the decrease in activity was significantly greater than zero, then the inhibition of the target enzyme was reported.

## Results

**Metabolite Profiling in Individual P450 Enzymes.** The metabolic profiles for 48 drugs were evaluated in 17 individual P450 enzymes using UHPLC-UV-HRMS (Fig. 2). This represents the first, "qualitative" step in the process, wherein any P450 enzymes with the capability to generate metabolites for a given drug are identified. For each drug, the enzymes were classified into one of three groups: 1) metabolites were generated and observed in the UV chromatogram, 2) metabolites were generated but only observed in the HRMS data, and 3) no metabolites were detected. Depicted in Fig. 2 are dark green boxes that indicate the generation of metabolites observed in the UV data (which are also observed in the more sensitive HRMS data) and pale green boxes that indicate the observation of metabolites observed only in the HRMS data. Within the entries on Fig. 2 are solid circles, which indicate that a particular P450 enzyme has been demonstrated to be involved in the clearance of the drug based on clinical pharmacokinetic data (either DDI data with a well-established P450-selective inhibitor or a difference in pharmacokinetics observed in subjects possessing different genetic polymorphisms for P450 enzymes). Among the 48 drugs evaluated, there were 87 instances of clinical evidence supporting meaningful contributions of specific P450 enzymes to the metabolism of a drug. In 84 of these cases, metabolites were observed in the UV data, and in the other three, metabolites were observed, but only in the HRMS data. In these latter three cases, the contributions are minor (CYP3A4 contributions to tolbutamide and venlafaxine clearance and CYP2E1 to warfarin clearance; O'Reilly, 1973; Krishnaiah et al., 1994; Lindh et al., 2003). Thus, there are no false negatives, i.e., every enzyme demonstrated to be contributing to the clearance of a drug in a clinically meaningful manner is identified in this approach.

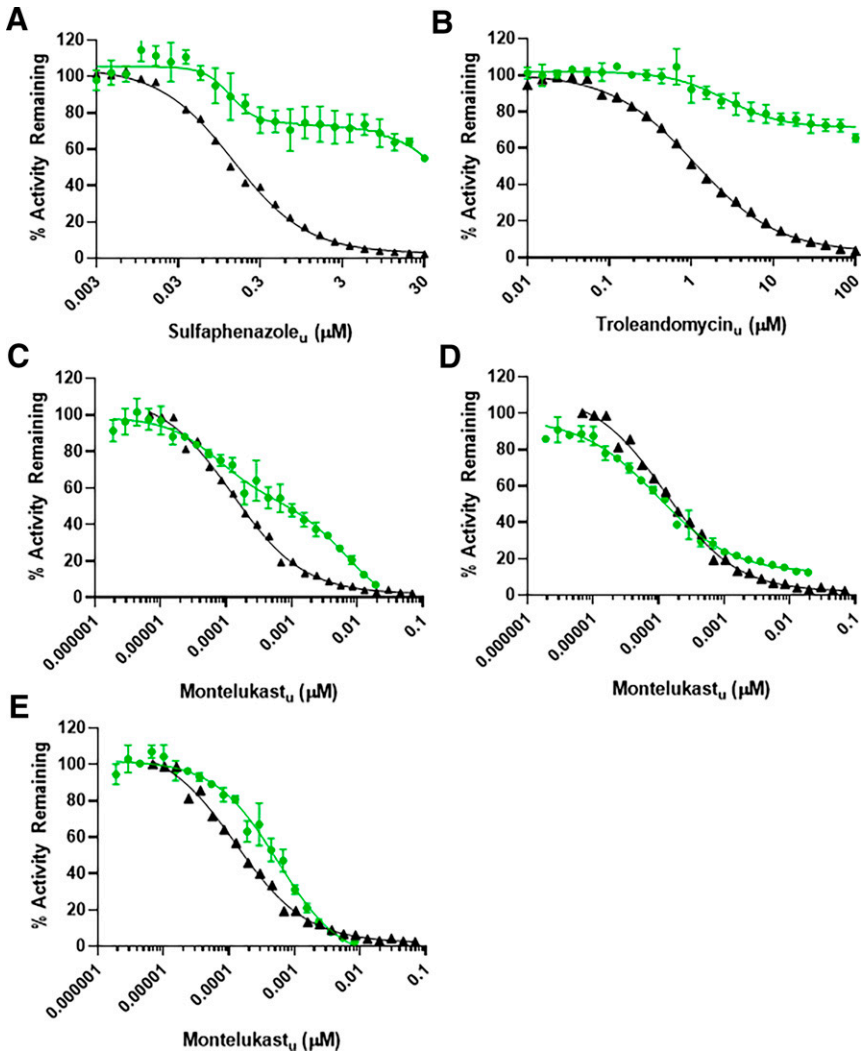


**Fig. 4.** Inhibition curves for metabolism of pioglitazone. (A) Effect of sulfaphenazole on 2-hydroxylation. (B) Effect of troleandomycin on 5-hydroxylation. (C–E) Effect of Montelukast on 2-. 1'-, and 2'-hydroxylation reactions, respectively. Green curves represent pioglitazone metabolism and black curves represent the positive control reactions for CYP2C9 (diclofenac 4'-hydroxylation), CYP3A (midazolam 1'-hydroxylation), and CYP2C8 (amodiaquine N-deethylation).

Also included in Fig. 2 are previous reports of any in vitro evidence of the involvement of a P450 enzyme in the metabolism of the 48 drugs, which are indicated with open circles. There are a total of 244 instances in which evidence has been reported, using various in vitro methods, that a P450 enzyme was claimed to be involved in the metabolism of a drug. Out of those, 242 were shown using the present approach. The only two not shown were reports of CYP2A6 catalyzed metabolism of atomoxetine (MacKenzie et al., 2020) and CYP2C8 catalyzed metabolism of lansoprazole (Pichard et al., 1995), neither of which has there been any report of clinical relevance.

In addition to the utility of these data in the qualitative-then-quantitative approach to identifying P450 enzymes involved in metabolic clearance of drugs, there are interesting trends that can be noted. The preponderance of CYP2C19 and CYP2D6 in drug metabolism is high (44 of 48 and 47 of 48, respectively). This is not aligned with the frequency of meaningful contributions of these enzymes to in vivo metabolic clearance, likely because in the experimental design employed (i.e., 100 pmol P450/mL) these enzymes are quantitatively over-represented. It is clear that CYP2A6, CYP4A11, and CYP4F2 are least frequently involved in metabolism (16, 17, and nine out of 48 drugs metabolized, respectively). CYP2B6 and CYP2E1 were each shown to metabolize 28 of the 48 drugs, however, in almost all cases this metabolism was detected only by HRMS data; when evaluated by UV data these two enzymes only readily metabolized nine and six drugs, respectively, out of the 48. As anticipated, with few exceptions, CYP3A enzymes were shown to be capable of metabolizing almost all of the drugs. But, unexpectedly, the frequency of CYP1A1, CYP1B1, and CYP2J2 being able to generate metabolites in high enough abundance for UV detection was high. Within the data, there were also instances of less-studied P450 enzymes being able to not only catalyze metabolism of certain drugs, but in high conversion (e.g., CYP3A7 metabolism of fluvastatin, CYP2J2 metabolism of linezolid, and CYP2C18 metabolism of warfarin, to name a few), which poses new questions regarding the possible impact of these enzymes on the pharmacokinetics of these drugs. Examples of the UV chromatograms for extracts of rCYP incubations for fluvastatin, pioglitazone, propranolol, risperidone, and escitalopram are shown in Supplemental Figs. 1–5.

**Fluvastatin: Enzyme Kinetics and Reaction Phenotyping.** Fluvastatin was metabolized to 5-hydroxy, 6-hydroxy, and N-desisopropyl metabolites in human liver microsomes (Fig. 1). Enzyme kinetic data yielded $CL_{int}$ values for these three pathways that resulted in calculated $f_{CL}$ values of 0.36, 0.42, and 0.21, respectively (Table 1; Supplemental Fig. 6). Single-concentration inhibitor data showed that the P450-selective inhibitors sulfaphenazole (CYP2C9), N-benzylnirvanol (CYP2C19), and TAO (CYP3A4) inhibited fluvastatin overall metabolism by 81%, 11%, and 24%, respectively (Table 2). These values compare favorably with the estimated in vivo contribution by CYP2C9 ($f_m$ = 0.76; Table 6), but overestimate the contribution by CYP3A4. Using the maximum percent

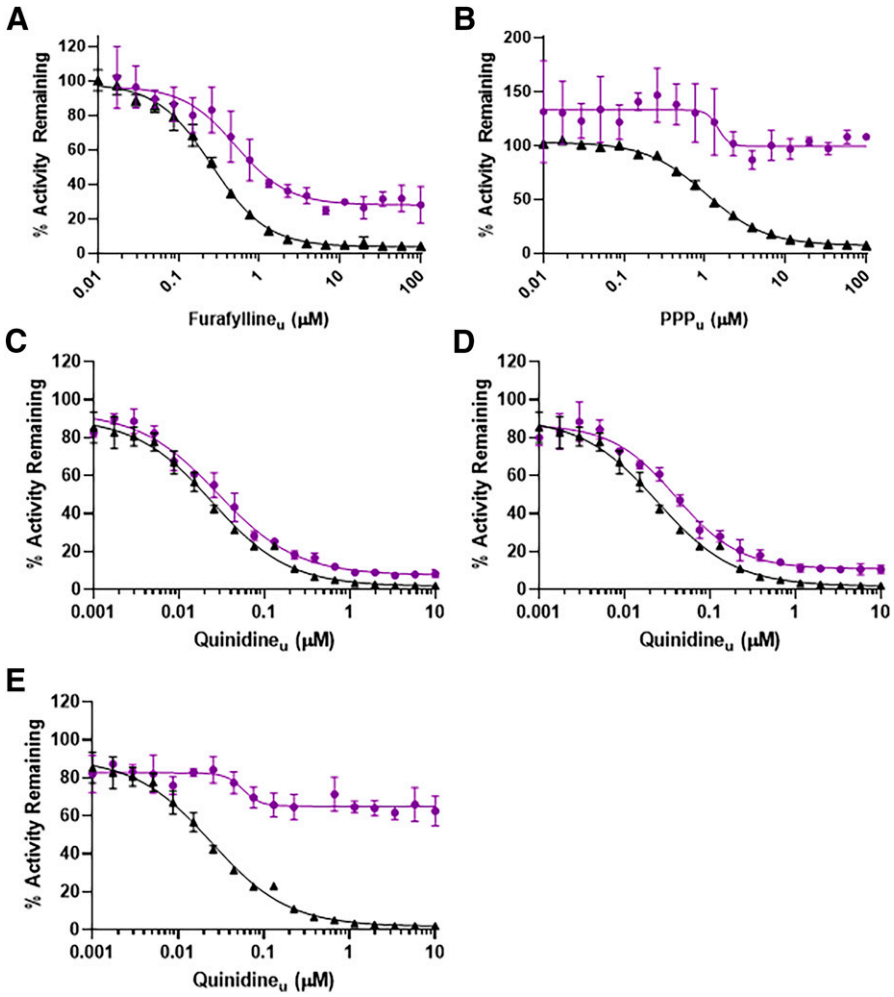


**Fig. 5.** Inhibition curves for metabolism of propranolol. (A) Effect of furafylline on N-dealkylation. (B) Effect of PPP on N-dealkylation. (C–E) Effect of quindine of 4-hydroxylation, 5-hydroxylation, and N-dealkylation reactions, respectively. Violet curves represent propranolol metabolism and black curves represent the positive control reactions for CYP1A2 (phenacetin O-dethylation), CYP2B6 (bupropion hydroxylation), and CYP2D6 (dextromethorphan O-demethylation).

inhibition values estimated from complex inhibition curve fitting (Fig. 3) yielded $f_m$ values of 0.76 and 0.15 for CYP2C9 and CYP3A4, respectively, while CYP2C19 was concluded to not contribute (Table 3). (It should be noted that in this instance a maximal effect on 5-hydroxylation was not reportable because of assay interference at high concentrations of TAO.)

Recombinant CYP2C8, CYP2C9, CYP2D6, and CYP3A4 were all demonstrated to metabolize fluvastatin at measurable rates (Supplemental Table 10). When adjusting the measured rates for the three reactions by ISEF values for these four enzymes (Table 4), $f_m$ values of 0.67, 0.29, 0.05, and <0.01 were determined for CYP2C9, CYP3A4, CYP2C8, and CYP2D6, respectively (Table 5). Thus, like the inhibition data, the estimated $f_m$ for CYP2C9 matches reasonably well the values estimated from in vivo pharmacogenetic data estimated for CYP2C9 (Table 6). However, the contribution of CYP3A4 is overestimated when compared with the clinical DDI study result ($f_m$ 0.12) shown in Table 6.

**Pioglitazone: Enzyme Kinetics and Reaction Phenotyping.** Pioglitazone was shown to be metabolized to four hydroxylated metabolites (Fig. 1), and these matched those that had been structurally characterized previously (Shen et al., 2003). Enzyme kinetic analysis of pioglitazone metabolism in human liver microsomes revealed that almost three-quarters of intrinsic clearance arises via 1'- and 2'-hydroxylation of the ethyl side chain (Table 1; Supplemental Fig. 7). Single-concentration inhibitor data supported that CYP2C8, CYP3A, CYP2C9, and CYP1A2 were involved in pioglitazone metabolism with estimated contributions of 0.60, 0.04, 0.04, and 0.04, respectively (Table 2). However, full curve data did not show a contribution from CYP1A2, but showed high involvement of CYP2C8 ($f_m$ = 0.72) along with small contributions from CYP2C9 and CYP3A4 (Table 3; Fig. 4).

Among rCYP enzymes, pioglitazone metabolites were generated by CYP1A2, CYP2C8, CYP2C9, and CYP3A4 (as above) but also CYP2C19 and CYP2D6 (Supplemental Table 10). However, correction of the rates by ISEF and abundance values resulted in an estimated $f_m$ for CYP2C8 of 0.82, with the other enzymes contributing very little (Tables 4 and 5). These values and those from inhibition data can be compared with an estimate of an in vivo value of 0.73 for CYP2C8, based on a gemfibrozil DDI study (Table 6). Thus, the main role for CYP2C8 was identified by all methods, albeit the inhibition curve approach yielded the estimate of $f_m$ that was closest (0.73 versus 0.72; Table 6).

**Propranolol: Enzyme Kinetics and Reaction Phenotyping.** Propranolol is metabolized by P450-catalyzed oxidations, as well as direct glucuronidation, thus the determination of $f_{CL}$ values required the use of pooled human hepatocytes to accommodate the glucuronidation reactions. Enzyme kinetics (Supplemental Fig. 8) of three oxidative reactions (4-hydroxylation, 5-hydroxylation, and N-deisopropylation), along with two glucuronidation reactions (O- and N-glucuronidations), are listed in Table 1 with estimated $f_{CL}$ values. (There was a fourth oxidative product, 7-hydroxypropranolol, however its $f_{CL}$ value was well under 0.01 and thus it was not measured in subsequent experiments.) 4-Hydroxylation is the dominant pathway ($f_{CL}$ = 0.77). The

glucuronidation reactions accounted for 18% of metabolism in hepatocytes, and this value must be accounted for when estimating $f_m$ values for the oxidation pathways when using liver microsomes and rCYPs. Single point inhibition data suggested a dominating role for CYP2D6 and a minor role for CYP1A2 (Table 3). Full inhibition curves (Fig. 5) showed roles for CYP1A2 and CYP2D6, as well as for CYP2B6 (in N-dealkylation only). Estimated $f_m$ values were 0.68, 0.03, and 0.02 for CYP2D6, CYP1A2, and CYP2B6, respectively. Notably, the minor role for CYP2B6 was revealed with the data-rich full inhibition curve, but the single point data for the effect of PPP on propranolol N-desisopropylation did not achieve statistical significance.

Propranolol metabolism was observed in several rCYPs when measuring metabolites with a sensitive HPLC-MS assay (Supplemental Table 10). Overall, when corrected for ISEF values, few of these enzymes were estimated to have a meaningful contribution to metabolism. The main contribution was from CYP2D6, which is in agreement with the inhibition data, albeit the estimated $f_m$ value was somewhat lower (0.55; Table 5) and was within the range of estimated in vivo $f_m$ values (Table 6). The lower CYP2D6 $f_m$ value estimated from rCYP data as compared with inhibition data are due to an observable contribution by CYP3A4 ($f_m$ = 0.11), which was not identified in TAO inhibition experiments in human liver microsomes. Furthermore, estimates of CYP3A contribution in vivo range as high as 0.39 from DDI data (Table 6), however, it is important to note that these DDI were observed with other drugs that affect cardiovascular functions (i.e., diltiazem and verapamil), and in one of those studies there was no effect observed on exposure to the 4-hydroxy metabolite, which would contradict CYP3A inhibition (since the 4-hydroxy metabolite was the major one formed by recombinant CYP3A4). Thus, the CYP3A4 contribution to propranolol clearance is unclear, but the CYP2D6 contribution was readily identified.

**Risperidone: Enzyme Kinetics and Reaction Phenotyping.** In human liver microsomes, risperidone was metabolized by three routes: 7-hydroxylation, 9-hydroxylation, and N-dealkylation (Fig. 1). For all three reactions, substrate saturation experiments showed biphasic kinetics (Supplemental Fig. 9). From the summed $CL_{int}$ data, the fraction of metabolic clearance progressing through the 7-hydroxy, 9-hydroxy, and N-dealkylation pathways were calculated at 0.16, 0.67, and 0.17, respectively (Table 1). Using data from single concentrations of P450-selective inhibitors, it was shown that risperidone was metabolized mostly by CYP2D6 and CYP3A4, with minor involvement of CYP2C8 and CYP2C19 (Table 2). Using the approach of complete inhibition curves (Fig. 6) and fitting the data to generate the maximum inhibition value showed that only CYP2D6 and CYP3A4 contribute, with $f_m$ values of 0.60 and 0.34, respectively (Table 3), which compare favorably to values estimated from pharmacogenetic and DDI studies (Table 6).

When using reaction rate data from rCYP enzymes, risperidone was shown to be metabolized by CYP2C8, CYP2C19, CYP2D6, and CYP3A4 (Supplemental Table 10). Adjusting each reaction rate using ISEF values (Table 4) and calculating $f_m$ values for these four enzymes yielded values of 0.07, 0.01, 0.19, and 0.73 for CYP2C8, CYP2C19, CYP2D6, and CYP3A4, respectively (Table 5). With this approach, CYP3A4 is overemphasized at the expense of CYP2D6 and these estimates of $f_m$ do not compare favorably with in vivo estimates (Table 6).

**Escitalopram: Enzyme Kinetics and Reaction Phenotyping.** Escitalopram is metabolized primarily via two routes at the amine nitrogen: N-demethylation and N-deamination, with the latter pathway initially yielding an aldehyde that undergoes rapid oxidation to a carboxylic acid (Fig. 1). Because of this latter pathway, the enzyme kinetics were measured in pooled human hepatocytes (Table 1; Supplemental Fig. 10) to generate $f_{CL}$ values of 0.80 and 0.20 for N-demethylation and N-deamination, respectively. Evaluation of inhibition data suggested roles for CYP2B6, CYP2C8, CYP2C19, CYP2D6, and CYP3A4 (Tables 2 and 3; Fig. 7). For the N-deamination reaction, inhibition data were generated using pooled human hepatocytes and showed essentially complete inhibition using the CYP2C19 inactivator esomeprazole. Also observed was a partial effect on N-demethylation, suggesting a role for CYP2C19 in this reaction as well. Initial data in human liver microsomes showed little to no effect of N-benzylnirvanol on escitalopram N-demethylation (Supplemental Fig. 11). The hepatocyte data showing a role for CYP2C19 in N-demethylation was aligned with the metabolite profile data in rCYP2C19 (Supplemental Fig. 5), and illustrates leveraging the knowledge gained from the initial qualitative rCYP metabolite profiling data when interpreting the inhibition data. The estimated in vivo

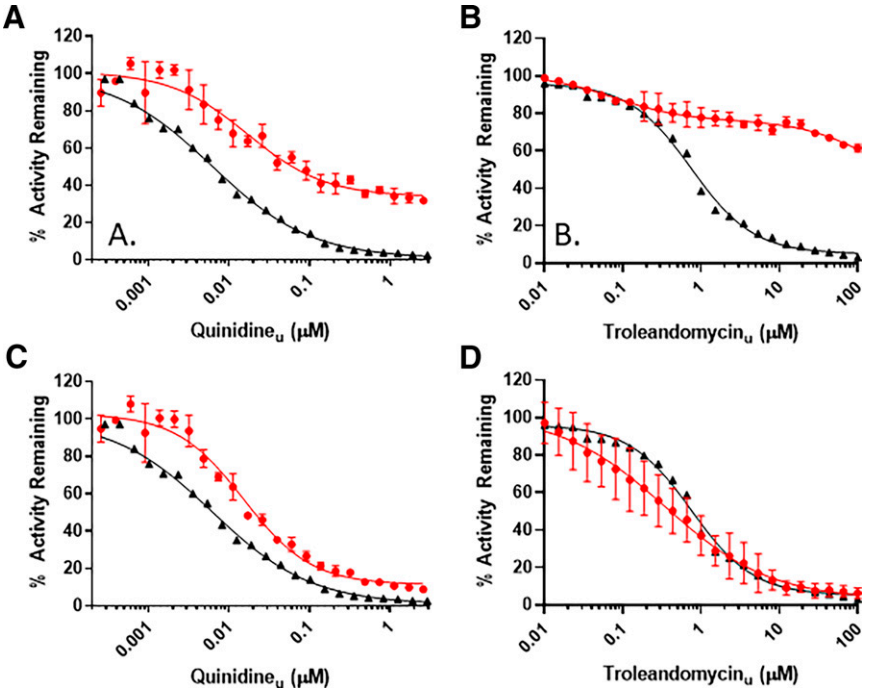


**Fig. 6.** Inhibition curves for metabolism of risperidone. (A and B) Effect of quinidine and troleandomycin on 9-hydroxylation. (C) Effect of quinidine on 7-hydroxylation. (D) Effect of troleandomycin on N-dealkylation. Red curves represent risperidone metabolism and black curves represent the positive control reactions for CYP2D6 (dextromethorphan O-demethylation), and CYP3A (midazolam 1'-hydroxylation).

values for CYP2C19 contribution to escitalopram clearance from pharmacogenetic studies give a wide range of 0.36–0.82 (Table 6) with a minor contribution from CYP3A and no impact of CYP2D6. Also shown in Fig. 7 is the inhibition curve generated by TAO, which is readily interpretable, and data can be fit to a simple four-parameter inhibition curve. Finally, it should be noted that monoamine oxidase inhibitors were also tested for their effect on escitalopram N-deamination in human hepatocytes, since a previous report described a role for monoamine oxidase in this reaction (Rochat et al., 1998). However, in the present study no effects of monoamine oxidase inhibitors chlorgyline (0.1 μM) or selegiline (1 μM) were observed. It is still possible that monoamine oxidase in extrahepatic tissues contributes to escitalopram clearance in vivo.

In rCYP enzymes, escitalopram N-demethylation was measurable in CYP1A2, CYP2C8, CYP2C19, CYP2D6, and CYP3A4, with CYP2D6 catalyzing this reaction at a very high rate relative to the others (Supplemental Table 10). Only CYP2C19 was able to generate the carboxylic acid metabolite. Following correction for ISEF factors for rate (Table 4), estimations of $f_m$ values for escitalopram total metabolism were 0.22, 0.23, 0.47, and 0.08 for CYP2C8, CYP2C19, CYP2D6, and CYP3A4, respectively, with the contribution by CYP1A2 less than 0.01 (Table 5). This may overemphasize the CYP2D6 contribution relative to CYP2C19, since not all of the enzymes may be able to convert an initial (and undetectable) aldehyde metabolite from N-deamination to the carboxylic acid, but several are able to catalyze formation of the readily detectable N-desmethyl metabolite.

## Discussion

The quantitative estimation of the involvement of individual P450 enzymes to metabolic clearance from in vitro data is important in drug research, as the data can inform the need for clinical drug interaction and pharmacogenetic studies. Two orthogonal approaches, effect of specific inhibitors in human liver microsomes or hepatocytes and ISEF-corrected metabolism rates in expressed P450 enzymes, have been recommended in consortia publications and regulatory guidance documents (Bjornsson et al., 2003; EMA, 2012; Bohnert et al., 2016; FDA, 2020: https://www.fda.gov/regulatory-information/search-fda-guidance-documents/in-vitro-drug-interaction-studies-cytochrome-p450-enzyme-and-transporter-mediated-drug-interactions). However, these approaches are not perfect. Selective inhibitors are generally not selective enough, especially when used at single-test concentrations (Lu, et al., 2003; Khojasteh et al., 2011; Nirogi et al., 2015; Doran et al., 2022). The use of rCYP enzymes can be flawed because different marker substrates can yield different ISEFs (Siu and Lai, 2017; Lindmark et al., 2018; Wang et al., 2019; Dantonio et al., 2022). The two methods can frequently yield $f_m$ values that are not in agreement. The objective of the present work was to develop an approach that would yield improved reaction phenotyping data.

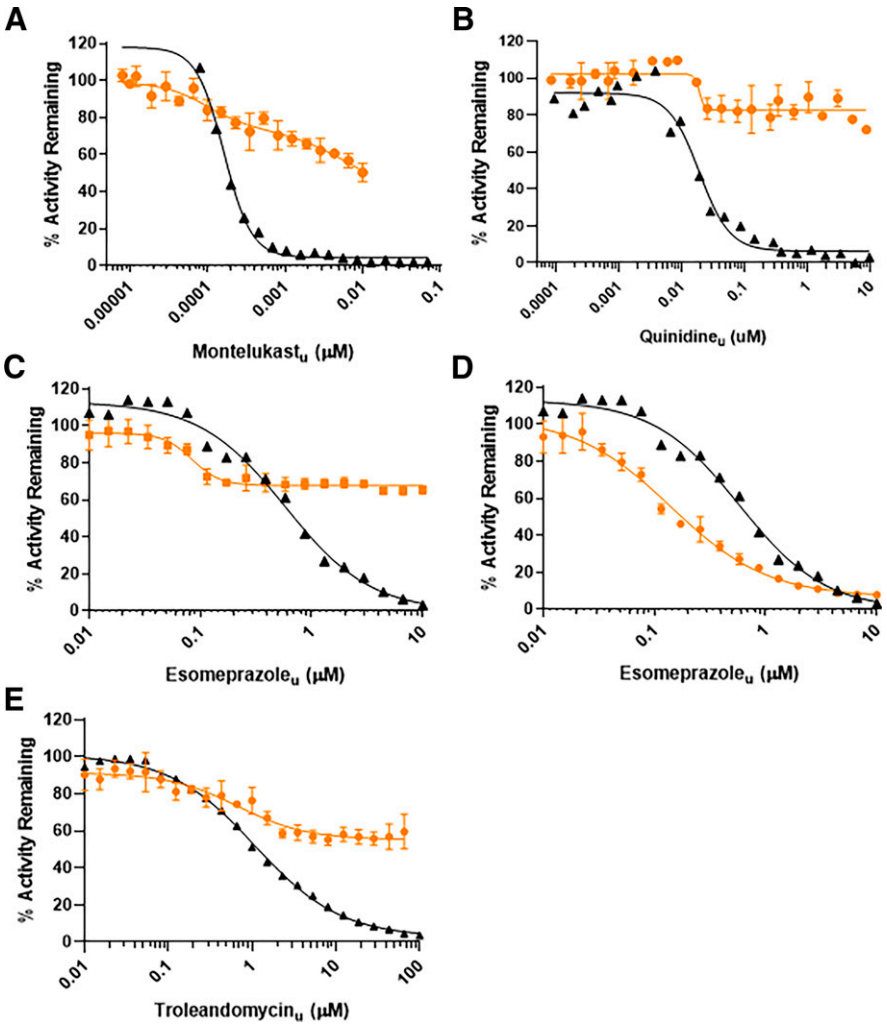


**Fig. 7.** Inhibition curves for metabolism of escitalopram. (A) Effect of montelukast on N-demethylation in human liver microsomes. (B) Effect of quindine on N-deamination in human liver microsomes. (C) Effect of esomeprazole on N-demethylation in human hepatocytes. (D) Effect of esomeprazole on N-deamination in human hepatocytes. (E) Effect of troleandomycin on N-demethylation in human liver microsomes. Orange curves represent escitalopram metabolism and black curves represent the positive control reactions for CYP2C8 (amodiaquine N-deethylation), CYP2D6 (dextromethorphan O-demethylation), CYP2C19 (mephenytoin 4'-hydroxylation), and CYP3A (midazolam 1'-hydroxylation).

Forty-eight drugs were first evaluated in baculosome-expressed rCYP enzymes using a metabolite profiling approach, and from this set, five were selected for detailed reaction phenotyping using both rCYPs with ISEF and selective inhibitors. These five were selected to ensure that the involvement of different P450 enzymes was evaluated and that they had commercially available or readily biosynthesized metabolite standards needed for quantitative bioanalysis. The estimated $f_m$ values were compared with those estimated from clinical DDI and pharmacogenetic studies (Table 6; Fig. 8). Overall, the use of chemical inhibitors using a full concentration range offered the values of $f_m$ that were closest to clinical data. The merits of this, when integrated into a "qualitative-then-quantitative" reaction phenotyping experimental design (Fig. 9), are described below.

Baculosome-expressed rCYPs are valuable reagents. Although it was not the main objective of the study, some interesting observations into these enzymes can be made from the data in Table 2. As expected, the P450 enzymes that have been a focus of drug metabolism for decades, such as CYP3A4, CYP3A5, CYP1A2, CYP2C8, CYP2C9, CYP2C19, and CYP2D6, show a high prevalence of ability to metabolize drugs (at least from this set of 48). But there were also some unexpected observations, such as the high frequency with which some of the less-studied enzymes, such as CYP1A1, CYP1B1, CYP2J2, CYP2C18, and CYP3A7, demonstrated an ability to catalyze drug metabolism. Some of these latter P450s are not highly expressed in the liver or are extrahepatically expressed. Also, at present, they do not have well-characterized selective inhibitors or marker substrate activities, which makes it difficult to understand their relative contributions to the in vivo metabolism of any given drug. However, despite the overall value of rCYPs in identifying the potential for involvement in metabolism, their use in making quantitative $f_m$ estimates is limited. For pioglitazone, fluvastatin, and propranolol, rCYPs with ISEFs yielded values in agreement with clinical data for their major clearing enzymes CYP2C8, CYP2C9, and CYP2D6, respectively. However, the contribution of CYP2D6 to risperidone metabolism was far underestimated, wherein the low $f_m$ value of 0.19 would not project the important impact of CYP2D6 expression on risperidone pharmacokinetics. A similar finding was made for escitalopram and CYP2C19. From examples like these and others (unpublished data on experimental drug candidates), we conclude that rCYP data

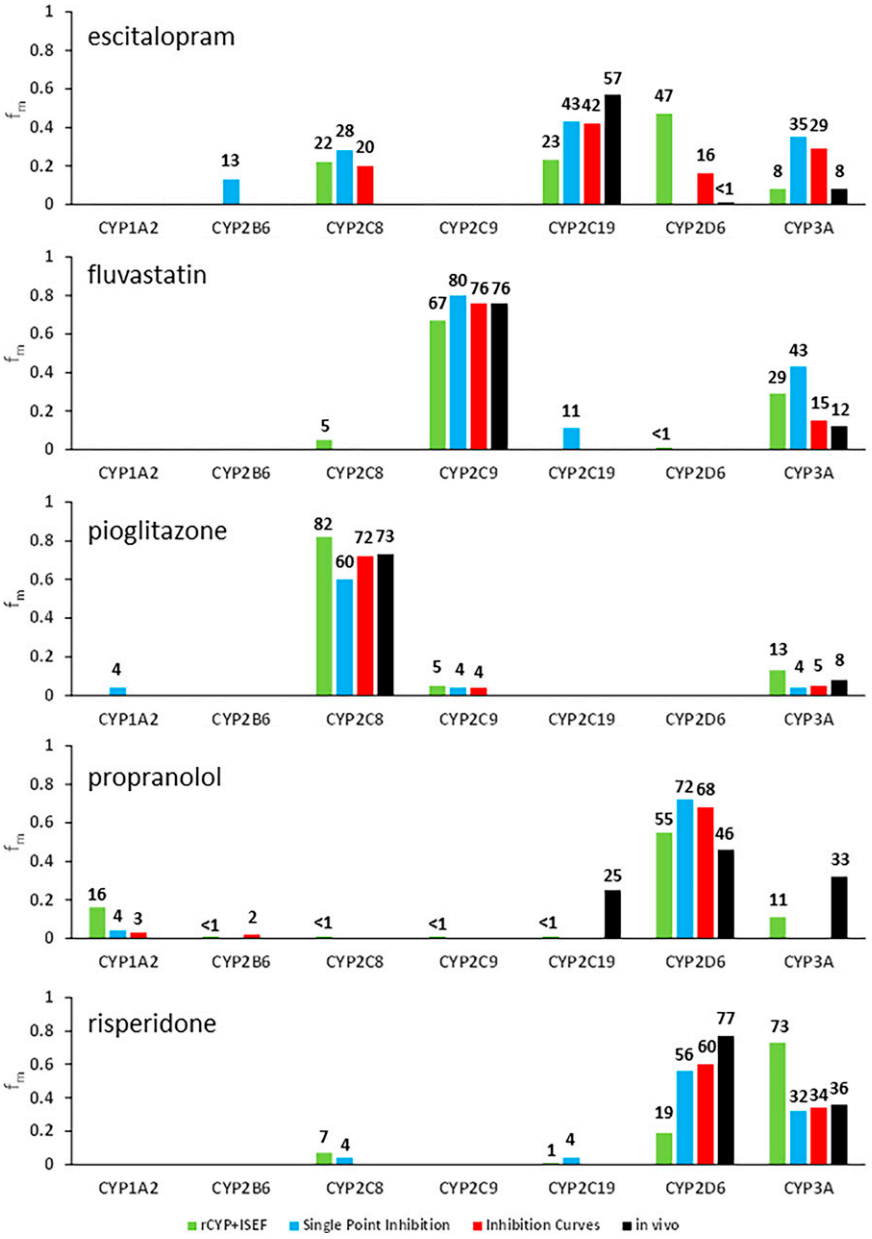


**Fig. 8.** Comparison of $f_m$ values calculated by different methods and in vivo estimates. For instances in which more than one clinical report was available the median value is shown.

should not be used quantitatively to project $f_m$ values. The observation that some ISEF values vary with the P450 marker substrates used to derive them is proposed as a main factor contributing to this problem (Siu and Lai, 2017; Lindmark et al., 2018; Wang et al., 2019; Dantonio et al., 2022). Reasons underlying substrate-dependent ISEF values at the biochemical level are unknown. However, it has been demonstrated that rCYPs can be useful in an initial qualitative assessment of metabolism, especially when combined with modern methods of metabolite profiling and identification. By following the formation of metabolites, rCYP incubations never failed to identify an enzyme that has importance in drug clearance for all 48 of the drugs evaluated (Fig. 2). In fact, this approach was too sensitive in many cases, as shown by numerous instances in which a given enzyme demonstrated a capability to generate metabolites for a drug even when the enzyme has no demonstrated clinical relevance. But there were no instances of false negatives where an enzyme important in clearance in vivo failed to generate metabolites. As such, this experiment can offer a good first step in a reaction phenotyping cascade (Fig. 9). Any P450 that demonstrates an ability to generate metabolites would move on to subsequent evaluation with inhibitors in liver microsomes (or hepatocytes).

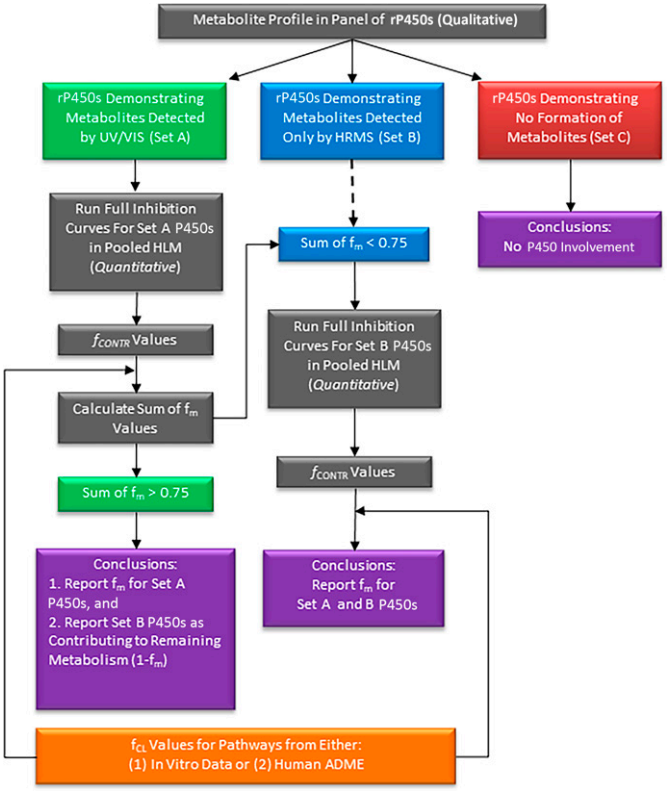


**Fig. 9.** Overall approach for P450 reaction phenotyping. A qualitative determination of metabolite profiles is conducted across a panel of individually expressed P450 enzymes using HPLC-UV-HRMS. Enzymes that yield no discernable metabolites by UV/VIS or HRMS are eliminated from any further consideration. Those enzymes that demonstrate formation of metabolites detected by UV/VIS are of greatest focus (Set A). Full inhibition curves are generated in human liver microsomes using inhibitors to address only Set A enzymes and generate $f_{CONTR}$ values. The $f_{CONTR}$ values are combined with $f_{CL}$ values, obtained from either quantitative metabolite profiles from human metabolism-excretion studies or from metabolite profile data generated in an appropriate in vitro system, to yield $f_m$ values. If the sum of $f_m$ values across all pathways exceeds 0.75, then the P450 phenotyping is considered complete, and any remaining uninhibited activity ($f_m$ < 0.25) is attributed to the enzymes that generated metabolites only detectable by HRMS (Set B). If the sum of $f_m$ values is less than 0.75, then additional inhibition curves are generated to yield $f_{CONTR}$ values for Set B P450 enzymes. In this latter case, the collective $f_m$ values for both Set A and Set B P450 enzymes are reported.

P450 inhibitors were evaluated in two ways: single concentration versus full inhibition curves. Use of single concentrations of inhibitors is commonly observed in literature reports describing P450 reaction phenotyping. A challenge with this lies in delineating a true contribution of a P450 versus spillover inhibition caused by suboptimal inhibitor selectivity (Doran et al., 2022). In Table 2, there are several instances of low but measurable inhibition, even cases where the standard deviation was lower than the percentage of inhibition. When summed, these small amounts of inhibition can erode the estimation of $f_m$ values for important enzymes. However, application of a more rigorous statistical evaluation (described in Materials and Methods) can eliminate these as artifacts.

To overcome problems of inhibitor spillover we employed a dense 18–22-point inhibition curve design for chemical inhibition experiments (seen in Figs. 3–7), which permits fitting complex functions to the data to reliably capture instances of nonselective inhibition. The power in this design affords a check on the inflection point of the first inhibition curve to verify agreement with the $IC_{50}$ for a known marker substrate activity, and also permits estimation of the maximum inhibition that is due only to effects on the target enzyme and excludes inhibition caused by spillover. Fraction metabolized values for the major P450 enzymes involved in the metabolism of the five example drugs were well-estimated using this approach. Success was realized particularly for escitalopram and risperidone, where the ISEF approach failed. Employing the most selective inhibitors is important. Finally, reaction phenotyping experimental designs, wherein the effects of inhibitors are assessed by measuring formation of metabolites, offer greater levels of sensitivity and granularity because the contribution of each enzyme to the formation of each metabolite is determined. Furthermore, it should be appreciated that following metabolite formation is essential for accurate reaction phenotyping of low intrinsic clearance drugs.

From the results of these studies, a "qualitative-then-quantitative" cascade approach is proposed for reaction phenotyping (Fig. 9). In step 1, a metabolite profile is generated for each rCYP enzyme. Those enzymes that yield the largest amounts of metabolites (especially observed in the UV traces) are selected for evaluation in step 2, which is a full multipoint inhibition curve for each of the enzymes identified in the first step. After step 2, if at least 75% of the total clearance is accounted for, then the study can be considered complete with the $f_m$ values reported from the maximum inhibition data, and the remaining $f_m$ (<25%) described as being catalyzed by a combination of the remaining P450s observed in step 1 and any other non-P450–mediated clearance. If less than 75% is accounted for, step 2 is expanded to the other P450s identified in step 1 that showed less metabolism (including those for which metabolites were only observed by MS). If an rCYP fails to generate any metabolites by MS, it can be concluded that the enzyme is not involved in the metabolism at all, since the first step yielded no instances of false negative outcomes. Such an approach leverages the value in each of the individual experiment types while avoiding their pitfalls.

In conclusion, a sequential "qualitative-then-quantitative" approach to P450 reaction phenotyping is proposed as an alternate to the current standard in-parallel two-orthogonal method approach described in reviews and guidance documents (Bjornsson et al., 2003; EMA, 2012; Bohnert et al., 2016; FDA, 2020: https://www.fda.gov/regulatory-information/search-fda-guidance-documents/in-vitro-drug-interaction-studies-cytochrome-p450-enzyme-and-transporter-mediated-drug-interactions). The approach merges metabolite profiling techniques into reaction phenotyping and leverages the best that each of the individual P450 reaction phenotyping tools have to offer while avoiding confounding factors such as inhibitor spillover and substrate-dependent ISEFs. Further efforts include investigation into roles for some of the P450 enzymes that are extrahepatically expressed, along with continued application of the qualitative-then-quantitative P450 phenotyping approach to drug candidates.

**Acknowledgments**

The authors express gratitude to Greg Steeno for discussion of statistical approaches, Raeanne Geffert for some preliminary data, and Greg Walker and Raman Sharma for qNMR data for biosynthesized metabolite standards.

**Authorship Contributions**

*Participated in research design:* Doran, Dantonio, Goosen, Obach.

*Conducted experiments:* Dantonio, Gualtieri, Balesano, Landers, Obach.

*Performed data analysis:* Doran, Dantonio, Gualtieri, Balesano, Landers, Burchett, Obach.

*Wrote or contributed to the writing of the manuscript:* Doran, Goosen, Obach.

**References**

Aquilante CL, Kosmiski LA, Bourne DW, Bushman LR, Daily EB, Hammond KP, Hopley CW, Kadam RS, Kanack AT, Kompella UB et al. (2013) Impact of the CYP2C8 *3 polymorphism on the drug-drug interaction between gemfibrozil and pioglitazone. *Br J Clin Pharmacol* **75**:217–226.

Bjornsson TD, Callaghan JT, Einolf HJ, Fischer V, Gan L, Grimm S, Kao J, King SP, Miwa G, Ni L et al.; Pharmaceutical Research and Manufacturers of America Drug Metabolism/Clinical Pharmacology Technical Working Groups (2003) The conduct of in vitro and in vivo drug-drug interaction studies: a PhRMA perspective. *J Clin Pharmacol* **43**:443–469.

Bohnert T, Patel A, Templeton I, Chen Y, Lu C, Lai G, Leung L, Tse S, Einolf HJ, Wang YH et al.; International Consortium for Innovation and Quality in Pharmaceutical Development (IQ) Victim Drug-Drug Interactions Working Group (2016) Evaluation of a New Molecular Entity as a Victim of Metabolic Drug-Drug Interactions-an Industry Perspective. *Drug Metab Dispos* **44**:1399–1423.

Byrne AJ, McNeil JJ, Harrison PM, Louis W, Tonkin AM, and McLean AJ (1984) Stable oral availability of sustained release propranolol when co-administered with hydralazine or food: evidence implicating substrate delivery rate as a determinant of presystemic drug interactions. *Br J Clin Pharmacol* **17**:45S–50S.

Cabaleiro T, Ochoa D, López-Rodríguez R, Román M, Novalbos J, Ayuso C, and Abad-Santos F (2014) Effect of polymorphisms on the pharmacokinetics, pharmacodynamics, and safety of risperidone in healthy volunteers. *Hum Psychopharmacol* **29**:459–469.

Dantonio AL, Doran AC, and Obach RS (2022) Intersystem extrapolation factors are substrate-dependent for CYP3A4: impact on cytochrome P450 reaction phenotyping. *Drug Metab Dispos* **50**:249–257.

Dimmitt DC, Yu DK, Elvin AT, Giesing DH, and Lanman RC (1991) Pharmacokinetics of diltiazem and propranolol when administered alone and in combination. *Biopharm Drug Dispos* **12**:515–523.

Doran AD, Dantoio AL, Gualtieri GM, Balesano A, Landers C, Burchett W, Goosen TC, and Obach RS (2022) Using a multiple concentration chemical inhibition design for improved reaction phenotyping. Manuscript submitted for publication.

EMA (2012) Guideline on the investigation of drug interactions.

Gassó P, Mas S, Papagianni K, Ferrando E, de Bobadilla RF, Arnaiz JA, Bioque M, Bernardo M, and Lafuente A (2014) Effect of CYP2D6 on risperidone pharmacokinetics and extrapyramidal symptoms in healthy volunteers: results from a pharmacogenetic clinical trial. *Pharmacogenomics* **15**:17–28.

Gelboin HV, Park SS, Fujino T, Song BJ, Cheng KC, Miller H, Robinson R, West D, and Friedman FK (1985) Cytochromes P-450, xenobiotic and endobiotic metabolism: monoclonal antibody directed detection, purification and reaction phenotyping, in *Proc. Int. Symp.* pp 390–401, Microsomes Drug Oxid.

Gutierrez MM, Rosenberg J, and Abramowitz W (2003) An evaluation of the potential for pharmacokinetic interaction between escitalopram and the cytochrome P450 3A4 inhibitor ritonavir. *Clin Ther* **25**:1200–1210.

Herrlin K, Yasui-Furukori N, Tybring G, Widén J, Gustafsson LL, and Bertilsson L (2003) Metabolism of citalopram enantiomers in CYP2C19/CYP2D6 phenotyped panels of healthy Swedes. *Br J Clin Pharmacol* **56**:415–421.

Jaakkola T, Backman JT, Neuvonen M, and Neuvonen PJ (2005) Effects of gemfibrozil, itraconazole, and their combination on the pharmacokinetics of pioglitazone. *Clin Pharmacol Ther* **77**:404–414.

Jukić MM, Haslemo T, Molden E, and Ingelman-Sundberg M (2018) Impact of CYP2C19 Genotype on Escitalopram Exposure and Therapeutic Failure: A Retrospective Study Based on 2,087 Patients. *Am J Psychiatry* **175**:463–470.

Khojasteh SC, Prabhu S, Kenny JR, Halladay JS, and Lu AY (2011) Chemical inhibitors of cytochrome P450 isoforms in human liver microsomes: a re-evaluation of P450 isoform selectivity. *Eur J Drug Metab Pharmacokinet* **36**:1–16.

Kirchheiner J, Kudlicz D, Meisel C, Bauer S, Meineke I, Roots I, and Brockmöller J (2003) Influence of CYP2C9 polymorphisms on the pharmacokinetics and cholesterol-lowering activity of (-)-3S,5R-fluvastatin and (+)-3R,5S-fluvastatin in healthy volunteers. *Clin Pharmacol Ther* **74**:186–194.

Kivistö KT, Kantola T, and Neuvonen PJ (1998) Different effects of itraconazole on the pharmacokinetics of fluvastatin and lovastatin. *Br J Clin Pharmacol* **46**:49–53.

Krishnaiah YS, Satyanarayana S, and Visweswaram D (1994) Interaction between tolbutamide and ketoconazole in healthy subjects. *Br J Clin Pharmacol* **37**:205–207.

Lennard MS, Jackson PR, Freestone S, Tucker GT, Ramsay LE, and Woods HF (1984) The relationship between debrisoquine oxidation phenotype and the pharmacokinetics and pharmacodynamics of propranolol. *Br J Clin Pharmacol* **17**:679–685.

Lindh JD, Annas A, Meurling L, Dahl ML, and AL-Shurbaji A (2003) Effect of ketoconazole on venlafaxine plasma concentrations in extensive and poor metabolisers of debrisoquine. *Eur J Clin Pharmacol* **59**:401–406.

Lindmark B, Lundahl A, Kanebratt KP, Andersson TB, and Isin EM (2018) Human hepatocytes and cytochrome P450-selective inhibitors predict variability in human drug exposure more accurately than human recombinant P450s. *Br J Pharmacol* **175**:2116–2129.

Lu AY, Wang RW, and Lin JH (2003) Cytochrome P450 in vitro reaction phenotyping: a re-evaluation of approaches used for P450 isoform identification. *Drug Metab Dispos* **31**:345–350.

MacKenzie KR, Zhao M, Barzi M, Wang J, Bissig K-D, Maletic-Savatic M, Jung SY, and Li F (2020) Metabolic profiling of norepinephrine reuptake inhibitor atomoxetine. *Eur J Pharm Sci* **153**:105488.

Mahatthanatrakul W, Sriwiriyajan S, Ridtitid W, Boonleang J, Wongnawa M, Rujimamahasan N, and Pipatrattanaseree W (2012) Effect of cytochrome P450 3A4 inhibitor ketoconazole on risperidone pharmacokinetics in healthy volunteers. *J Clin Pharm Ther* **37**:221–225.

McCourty JC, Silas JH, Tucker GT, and Lennard MS (1988) The effect of combined therapy on the pharmacokinetics and pharmacodynamics of verapamil and propranolol in patients with angina pectoris. *Br J Clin Pharmacol* **25**:349–357.

McLean AJ, Skews H, Bobik A, and Dudley FJ (1980) Interaction between oral propranolol and hydralazine. *Clin Pharmacol Ther* **27**:726–732.

Nagar S, Argikar UA, and Tweedie DJ (2014) Enzyme kinetics in drug metabolism: fundamentals and applications. *Methods Mol Biol* **1113**:1–6.

Nirogi R, Palacharla RC, Uthukam V, Manoharan A, Srikakolapu SR, Kalaikadhiban I, Boggavarapu RK, Ponnamaneni RK, Ajjala DR, and Bhyrapuneni G (2015) Chemical inhibitors of CYP450 enzymes in liver microsomes: combining selectivity and unbound fractions to guide selection of appropriate concentration in phenotyping assays. *Xenobiotica* **45**:95–106.

O'Reilly RA (1973) Interaction of sodium warfarin and disulfiram (antabuse) in man. *Ann Intern Med* **78**:73–76.

Parkinson A (1996) An overview of current cytochrome P450 technology for assessing the safety and efficacy of new materials. *Toxicol Pathol* **24**:48–57.

Pichard L, Curi-Pedrosa R, Bonfils C, Jacqz-Aigrain E, Domergue J, Joyeux H, Cosme J, Guengerich FP, and Maurel P (1995) Oxidative metabolism of lansoprazole by human liver cytochromes P450. *Mol Pharmacol* **47**:410–418.

Raghuram TC, Koshakji RP, Wilkinson GR, and Wood AJ (1984) Polymorphic ability to metabolize propranolol alters 4-hydroxypropranolol levels but not beta blockade. *Clin Pharmacol Ther* **36**:51–56.

Rochat B, Kosel M, Boss G, Testa B, Gillet M, and Baumann P (1998) Stereoselective biotransformation of the selective serotonin reuptake inhibitor citalopram and its demethylated metabolites by monoamine oxidases in human liver. *Biochem Pharmacol* **56**:15–23.

Rodrigues AD (1999) Integrated cytochrome P450 reaction phenotyping: attempting to bridge the gap between cDNA-expressed cytochromes P450 and native human liver microsomes. *Biochem Pharmacol* **57**:465–480.

Rowland M and Matin SB (1973) Kinetics of drug-drug interactions. *Journal of Pharmacokinetics and Biopharmaceutics* **1**:553–567.

Rudberg I, Mohebi B, Hermann M, Refsum H, and Molden E (2008) Impact of the ultrarapid CYP2C19*17 allele on serum concentration of escitalopram in psychiatric patients. *Clin Pharmacol Ther* **83**:322–327.

Rudberg I, Reubsaet JL, Hermann M, Refsum H, and Molden E (2009) Identification of a novel CYP2C19-mediated metabolic pathway of S-citalopram in vitro. *Drug Metab Dispos* **37**:2340–2348.

Shen Z, Reed JR, Creighton M, Liu DQ, Tang YS, Hora DF, Feeney W, Szewczyk J, Bakhtiar R, Franklin RB et al. (2003) Identification of novel metabolites of pioglitazone in rat and dog. *Xenobiotica* **33**:499–509.

Siu YA and Lai WG (2017) Impact of Probe Substrate Selection on Cytrochrome P450 Reaction Phenotyping Using the Relative Activity Factor. *Drug Metab Dispos* **45**:183–189.

Spence JD, Munoz CE, Hendricks L, Latchinian L, and Khouri HE (1995) Pharmacokinetics of the combination of fluvastatin and gemfibrozil. *Am J Cardiol* **76**:80A–83A.

Tateishi T, Nakashima H, Shitou T, Kumagai Y, Ohashi K, Hosoda S, and Ebihara A (1989) Effect of diltiazem on the pharmacokinetics of propranolol, metoprolol and atenolol. *Eur J Clin Pharmacol* **36**:67–70.

Tateishi T, Ohashi K, Fujimura A, and Ebihara A (1992) The influence of diltiazem versus cimetidine on propranolol metabolism. *J Clin Pharmacol* **32**:1099–1104.

Tsuchimine S, Ochi S, Tajiri M, Suzuki Y, Sugawara N, Inoue Y, and Yasui-Furukori N (2018) Effects of Cytochrome P450 (CYP) 2C19 Genotypes on Steady-State Plasma Concentrations of Escitalopram and its Desmethyl Metabolite in Japanese Patients With Depression. *Ther Drug Monit* **40**:356–361.

Waade RB, Hermann M, Moe HL, and Molden E (2014) Impact of age on serum concentrations of venlafaxine and escitalopram in different CYP2D6 and CYP2C19 genotype subgroups. *Eur J Clin Pharmacol* **70**:933–940.

Walker GS, Bauman JN, Ryder TF, Smith EB, Spracklin DK, and Obach RS (2014) Biosynthesis of drug metabolites and quantitation using NMR spectroscopy for use in pharmacologic and drug metabolism studies. *Drug Metab Dispos* **42**:1627–1639.

Wang S, Tang X, Yang T, Xu J, Zhang J, Liu X, and Liu L (2019) Predicted contributions of cytochrome P450s to drug metabolism in human liver microsomes using relative activity factor were dependent on probes. *Xenobiotica* **49**:161–168.

Ward SA, Walle T, Walle UK, Wilkinson GR, and Branch RA (1989) Propranolol's metabolism is determined by both mephenytoin and debrisoquin hydroxylase activities. *Clin Pharmacol Ther* **45**:72–79.

Yoshida K, Maeda K, and Sugiyama Y (2013) Hepatic and intestinal drug transporters: prediction of pharmacokinetic effects caused by drug-drug interactions and genetic polymorphisms. *Annu Rev Pharmacol Toxicol* **53**:581–612.

Yasuhara M, Yatsuzuka A, Yamada K, Okumura K, Hori R, Sakurai T, and Kawai C (1990) Alteration of propranolol pharmacokinetics and pharmacodynamics by quinidine in man. *J Pharmacobiodyn* **13**:681–687.

Zhou HH, Anthony LB, Roden DM, and Wood AJ (1990) Quinidine reduces clearance of (+)-propranolol more than (-)-propranolol through marked reduction in 4-hydroxylation. *Clin Pharmacol Ther* **47**:686–693.

**Address correspondence to:** R. Scott Obach, Pfizer Inc., Eastern Point Road, Groton, CT, 06340. E-mail: r.scott.obach@pfizer.com